ACTIVE FIRE DETECTION USING REMOTE SENSING BASED POLAR-ORBITING AND GEOSTATIONARY OBSERVATIONS: AN APPROACH TOWARDS NEAR REAL-TIME FIRE MONITORING

SUSAN PHILIP

MARCH, 2007

Course Title:	Geo-Information Science and Earth Observation for Environmental Modelling and Management
Level:	Master of Science (M.Sc)
Course Duration:	September 2005 - March 2007
Consortium partners:	University of Southampton (UK) Lund University (Sweden) University of Warsaw (Poland) International Institute for Geo-Information Science and Earth Observation (ITC) (The Netherlands)
GEM thesis number:	2005-28

ACTIVE FIRE DETECTION USING REMOTE SENSING BASED POLAR-ORBITING AND GEOSTATIONARY OBSERVATIONS: AN APPROACH TOWARDS NEAR REAL-TIME FIRE MONITORING

BY

SUSAN PHILIP

Thesis submitted to the International Institute for Geo-information Science and Earth Observation in partial fulfilment of the requirements for the degree of Master of Science in Geo-information Science and Earth Observation, Specialisation: (Environmental modelling and management)

Thesis Assessment Board

Chairman:	Dr. Ir. C.A.J.M. Kees de Bie
External Examiner	Prof. Peter Atkinson, University of Southampton, UK
First supervisor	Dr. B.H.P. Ben Maathuis
Second supervisor	Dr. Ir. C.A.J.M. Kees de Bie
Member	Prof. Katarzyna Dabrowska, University of Warsaw's Institute of Geodesy and Cartography, Poland

ITC International Institute for Geo-Information Science and Earth Observation, Enschede, The Netherlands

Disclaimer

This document describes work undertaken as part of a programme of study at the International Institute for Geo-information Science and Earth Observation. All views and opinions expressed therein remain the sole responsibility of the author, and do not necessarily represent those of the institute.

I certify that although I have conferred with others in preparing for this assignment, and drawn upon a range of sources cited in this work, the content of this thesis report is my original work.

Susan Philip

DEDICATED TO MY LOVING PARENTS

JOSEPH PHILIP AND KATHLEEN PHILIP

Abstract

Forest fires have drawn a lot of attention in recent years due to its effect on climate change and the ecosystem. Fire detection in real-time is a necessity to avoid large scale losses. Remote sensing is a quick and cheap technique for detecting and monitoring forest fires on a large scale. AVHRR has been used already for a long period for fire detection. The use of MODIS for fire detection has recently preceded AVHRR and a large number of fire products are being developed. The launch of MSG SEVIRI on August 2002 provides a unique opportunity to detect and monitor forest fires in real-time by providing images at 15 minutes interval. This work presents a comparison between the polar orbiting and geo-stationary satellites namely MSG, MODIS and AVHRR for detecting forest fires. Fire detection algorithms were designed for detecting forest fires with MSG, AVHRR and MODIS satellite sensors. The principle of the approach is to detect fires by comparing the observed TOA brightness temperature of the pixel with the expected temperature during fire conditions. The expected temperature is modelled by series of observations and the end product is a thresholding algorithm developed separately for MSG, MODIS and AVHRR. The satellite detected fire pixels were validated with ground data. The MSG SEVIRI has proved itself to be most suitable for detecting fires in real time as compared to MODIS and AVHRR. MSG has detected 88% of all the fires with an omission rate of 12%; MODIS detected 64% of all fires with an omission rate of 34 %; The performance of AVHRR was most unsatisfactory since AVHRR detected 37% of the total fires with an omission rate of 62%. Forest fires is a dynamic phenomenon and it is useful to have images for the entire day for proper real-time fire detection and therefore geostationary satellites are best suited for this purpose.

Acknowledgements

My first appreciation goes to the EU Erasmus Mundus consortium (University of Southampton, UK; University of Lund, Sweden; Warsaw University, Poland and ITC, The Netherlands) for awarding me a scholarship to pursue this programme in 4 European countries. This has been a wonderful experience for me. I express my gratitude towards all the teachers and staff of this M.Sc programme.

I am most grateful to my primary supervisor Dr. Ben Maathuis for his continuous, guidance; encouragement and patience from the beginning of this research work untill the production of this thesis. I have gained a lot of scientific knowledge from him, and I shall always remember and be grateful for his contribution in this research work. I would love to work with him in future. I am also grateful to my secondary supervisor Dr. Kees De Bie for his hard work, support and patience for field work preparation, field work data collection, and critical guidance during thesis writing. My sincere thanks Ir. V. Bas Retsios (Software Developer, ITC) for his kind support and help with the various softwares and for his renovative ideas in dealing with the data. He has a big contribution in making this research work a success.

I would like to thank the individual organization members in Portugal who have helped me with field data. In this regard I must mention Rui Natario (National Service for fire and civil protection in Santarem district, Portugal) for his kind help with necessary data and information. I express my deepest gratitude to his continuous help, patience and kindness. I would also like to express my gratitude towards Nuno Touret, Paulo Reis, Sandra Loureiro, Jacinta Perreira (Municipal coorperation in Ourem, Portugal), the forest department in Macao, Portugal, National Service for fire and civil protection in Leiria district, and Bombeiros in the different locales of Santarem and Leiria district. I would also like to thank my classmates and friends for their critical comments on my research work and their friendly support during my stay in ITC.

Table of contents

List of figures

List of tables

Acronyms and Abbreviations

AVHRR	Advanced Very High Resolution Radiometer
EOS	Earth Observing System
EUMETSAT	European Organisation for the Exploitation of Meteorological Satellites
GOES	Geostationary Operational Environmental Satellites
GPS	Global Positioning System
HRV	High resolution visible
MODIS	Moderate Resolution Imaging Spectroradiometer
MSG	Meteosat Second Generation
SEVIRI	Spinning Enhanced Visible and Infrared Imager Visible and Infrared Imager
WGS 84	World Geodetic System 1984

1. INTRODUCTION

Forest fires are natural phenomena which occur regularly on this earth, the scale may range from small fires with little impacts to very large fires having serious large scale impacts. This is an area of research which is experiencing an increase in attention by researchers over the years. It is necessary to locate the active fire burning areas since this is important for a number of other studies, like landuse and landcover change, it contributes in assessing the area and quantity of forests that are destroyed and further helps in wildlife management. It is useful for planning, management and prevention of future fire hazards and helps in prediction of fires or making a fire risk analysis. Fires release a lot of heat, smoke and aerosol particles into the atmosphere, this has very significant effects on the climate, and have been an area of interest for scientist dealing with climate change and this makes fire detection also useful for climatologists. Therefore, it maybe said that monitoring and detection of fires are useful in understanding the losses of man ecologically, economically and the losses socially. The problem has become more serious than years before. With growing of population Man has encroached over forest areas and has been the major cause in triggering forest fires. Climate unfortunately plays an important role in making the conditions favourable for the forest fires to occur. Drought conditions trigger fire, and if there is a lot of wind it can make a small fire extremely disastrous.

Remote sensing helps to provide information regularly over a large area. It helps in providing information for many research questions and problems of Man and one among them being detection and monitoring of forest fires. However, detection of fire with the help of satellite data also has many limitations. If there is a cloud then the fire cannot be thermally detected, the same problem would be if there is very thick smoke. It is necessary that the satellite overpasses the area during the fire time. In case of fire detection with brightness temperatures the added disadvantage is that there maybe false alarms from a number of objects, for example heated sand, and it may seem that there is a fire. Remote sensing though has many limitations is yet a benefit for fire detection since it is a cheap way to get information regularly over large area, which could be of tremendous importance in areas which are cursed by regular fires for example the Mediterranean region in Europe.

The satellite sensors useful for fire detection maybe geostationary and polar orbiting. Since 1980 the VAS instruments on GOES 4-7 has been used for fire monitoring.

GOES is a geostationary satellite. The spatial coverage from GOES included America (north, central and south), therefore the METEOSAT satellites was launched which included countries of Europe and Africa (Kaufman et al., 1998). The first generation Meteosat satellites included 7 Meteosat satellites that recorded 3 spectral regions (visible, infrared and water vapour regions of the electromagnetic spectrum) and imaged the Earth every 30 minutes. The Meteosat second Generation satellites (MSG) are more advanced than the Meteosat first generation satellites and will operate untill 2018. The MSG functions in 12 spectral bands with the help of its radiometer 'the Spinning Enhanced Visible and Infrared Imager (SEVIRI), and images the Earth every 15 minutes, at a spatial resolution of 3km at nadir for the SWIR and TIR bands, the HRV has a sampling distance of 1 km at sub-satellite point. The first MSG was Meteosat-8 which was launched in 2002; the second satellite was launched in December, 2005 (www.eumetsat.int).

The polar orbiting satellites which are most commonly used for fire monitoring are the NOAA AVHRR and MODIS. The AVHRR is jointly managed by The National Oceanic and Atmospheric Administration (NOAA) and the National Aeronautics and Space Administration (NASA). The TIROS-N was launched in October 1978. Then the NOAA-L and NOAA-M followed, and NOAA-4 and NOAA-6 was launched in December 1994. In1998, a new series of NOAA Polar Operational Environmental Satellites (POES) was launched called the NOAA-K. The Advanced Very High Resolution Radiometer (AVHRR) is a scanning radiometer. The first AVHRR carried on TIROS-N (1978) was 4-channel radiometer, AVHRR/2 was improved to 5 channels and AVHRR/3 is a channel 6 instrument carried in NOAA-15 (launched in 1998), it functions in a wide spectral range covering 0.65 micron to 11.9 micron wavelengths, and has a spatial resolution of 1.1km at nadir (Goodrum et al., 2000). The Moderate Resolution Imaging Spectroradiometer (MODIS) is on-board the Terra and Aqua satellites. Terra is managed by NASA's Goddard Space Flight Center and is multi-national, multi-disciplinary mission involving many partners. The Aqua is an integral part of the Earth Observing System (EOS) which is centred at NASA. EOS Terra satellite was launched on December 18, 1999, and Aqua Satellite was launched on May, 2002. MODIS images the Earth in 36 spectral bands ranging from 0.4 micron to 14.4 micron. The spatial resolution for the SWIR and TIR bands of MODIS is 1 km at nadir. The satellites Terra and Aqua operate at an altitude of 705 km in a sun-synchronous orbit (http://modis.gsfc.nasa.gov/). The most recent polar orbiting satellite is the meteorological operational (MetOp-A) satellite, which is a joint effort by EUMETSAT and NOAA; it was launched on October 19, 2006. The satellite flies at an orbit which is sun synchronous and at an altitude of 800-850 km. The MetOp has a number of instruments for meteorological observations.

However, the AVHRR/3 products of MetOp were not available when the author began working on this thesis (http://www.eumetsat.int).

The polar orbiting satellites operate at lower altitudes of around 800 km however; the disadvantage is that the same area is viewed only twice a day. The MODIS and NOAA AVHRR have a lower temporal resolution, MODIS gives four images for a particular location per day, which incase of NOAA AVHRR is 2 images per day. Geostationary satellites operate at an altitude of about 36,000 km above Earth. The revolution time of the geostationary satellites is same as the Earth therefore the satellites always view the same area. The MSG has a higher temporal resolution therefore gives a larger number of images per day which is very beneficial for studies involving rapidly changing phenomenon like monitoring of forest fires. However, the spatial resolution of MSG (except HRV channel) is much lower than NOAA AVHRR and MODIS since it is operating from a higher altitude. Therefore, MSG, NOAA AVHRR and MODIS have some benefits and limitations for detecting and monitoring forest fires and this research would compare the performance of the 3 satellite sensors.

1.1 PROBLEM STATEMENT

Forest fires can become very disastrous after 15-20 minutes of burning if the fuel and atmospheric conditions are right and therefore, it is necessary to detect forest fires as quick as possible. Most of the fire research in the past is limited to fire mapping of the burnt area but it is necessary to detect fires in real time so that the fires maybe tackled as soon as possible and prevent massive losses. It is necessary to have fire alert systems. A number of techniques are being used for fire detection, like airborne fire detection where people observe large areas during the flight and a GPS for location information. Another method is the watch tower from where large areas can be viewed. However the most efficient, easy and cost effective way is possible with the help of remote sensing.

There is a problem in choosing the most appropriate sensor for fire mapping. Different sensors have different observational abilities, having different spectral, radiometric, spatial and temporal resolutions. The Landsat Enhanced Thematic Mapper (ETM) has a high spatial resolution of 30m (SWIR) and 60m (TIR) however, its spatial coverage is small and it has a low temporal resolution such that most portions of the earth would get a good image once every 16 days (www.landsat.org). The ASTER (Advanced Space borne Thermal Emission and Reflection Radiometer), is carried on the Terra satellite and has a spatial resolution of 15m (VNIR), 30m (SWIR) and 90m (TIR), however, it has a overpass return

cycle of 16 days and therefore its temporal resolution is Aster's limitation to detected and monitor active fires (http://asterweb.jpl.nasa.gov). MSG on the other hand images the earth every 15 minutes. It covers of Europe and part of Africa with a spatial resolution of 3 km sub-satellite and lower spatial resolutions away from sub-satellite pixels. AVHRR/3 radiometer has a spatial resolution of 1 km and provides 2 images for a location, (day and night time image) and has been very popular in fire detection since it has a good balance in spatial resolution and revisit time. MODIS is a more recent satellite and has 36 bands in a wide spectral range. MODIS records images twice during the day and twice during the night and has a spatial resolution of 1 km (SWIR and TIR channels). The polar orbiting satellites partially fulfill the needs of fire detection since they produce 2-4 images for a place each day at relatively long temporal intervals which is not good for detecting fire in real time. MSG is best suited for real-time fire detection considering its high temporal resolution but MSG has the problem of low spatial resolution. Considering the strengths and weaknesses of the polar-orbiting and geostationary observations it is necessary to apply them together for fire detection. Since 1980s over the past few years there are many proposed algorithms for detecting fires. There are many national and international organizations which are actively engaged in detection of forest fires. For instance to mention a few: GOFC/GOLD Fire programme aims to develop a geostationary fire monitoring system (Prins, 2004). Modis has also formed a fire team and produces a number of fire products. The International Geosphere–Biosphere Programme (IGBP) approaches the fire issue from a multidisciplinary perspective, and has many projects for fire study. The International Global Atmospheric Chemistry (IGAC) project requires knowing how much forest is burnt so that it can study impacts on the atmosphere. The Global Climate and Terrestrial Ecosystems (GCTE) project studies the role of fire in the ecosystem. The Global Analysis Interpretation and Modelling (GAIM) project studies needs fire information to study its impact on the biogeochemical cycle reservoirs and fluxes (Stroppiana et al., 2000).

There is a lot of research being conducted to get the most appropriate method for active fire detection and this research focuses on the brightness temperatures anomaly detection method. There is however no perfect algorithm and the problems of omissions and commissions still persist. Majority of the fire detection algorithms have been applied to polar-orbiting satellites and the GOES geostationary satellites. Fire detection with MSG SEVIRI is not yet popular. The first trial fire products of MSG SEVIRI are now released on the METEOSAT website but quality of the product is not known yet. No information is available on the algorithm which they have used for fire detection. This study has decided to use 3 satellite sensors for fire

detection and monitoring. Two of the satellite sensors are polar orbiting; they are the NOAA-AVHRR/3 and MODIS, and the third being a geostationary satellite sensor, the Meteosat Second Generation (MSG) Spinning Enhanced Visible and Infrared Imager Visible and Infrared Imager (SEVIRI) instrument. Figure 1.1 gives an outline of the research issues dealt with in this thesis.

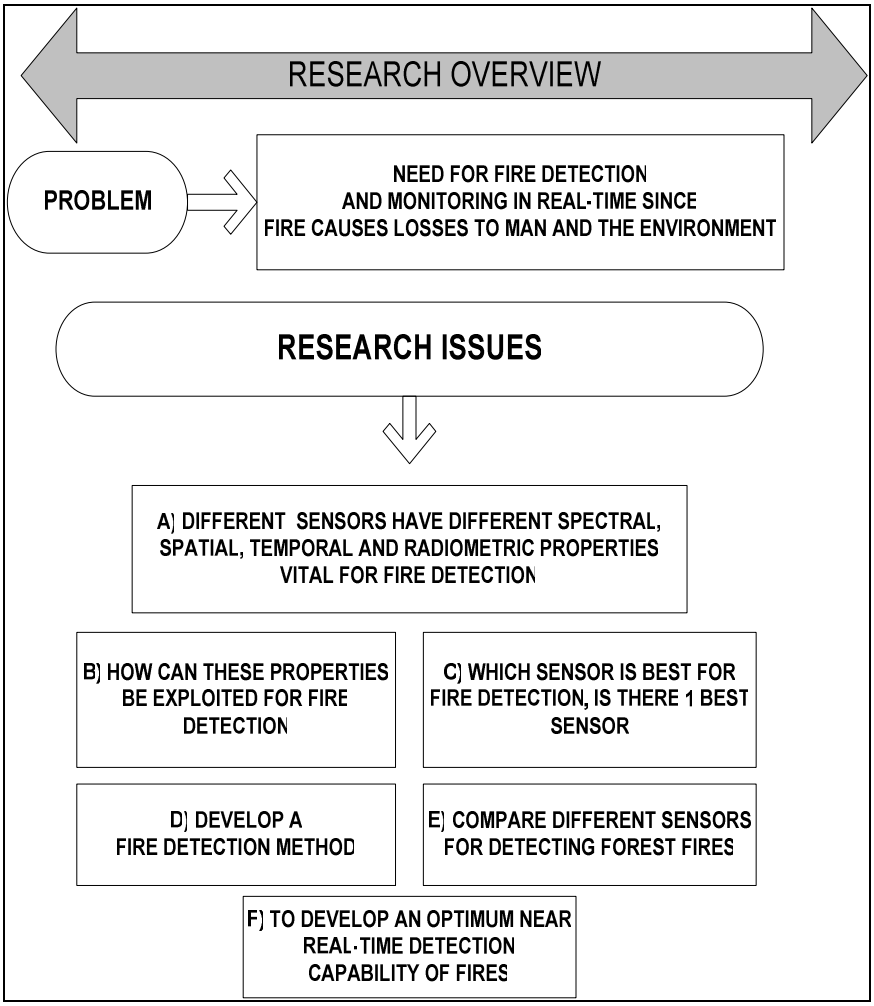

Figure 1.1 Overview of the research

1.2 RESEARCH OBJECTIVES AND QUESTIONS

The research aims to develop an approach to fire detection in near real-time using geo-stationary and polar orbiting satellite observations. This research uses 1 geostationary satellite and 2 polar orbiting satellites for detection of forest fires. The specific objectives and research questions are as follows:

SPECIFIC OBJECTIVES	**RESEARCH QUESTIONS**
1) To analyse the best bands for fire detection by comparing the sensitivity of different spectral regions to hotspots.	1) Which are the most suitable bands for detecting forest fires (MSG, MODIS and AVHRR)?
2) To develop an algorithm for MSG SEVERI, MODIS and AVHRR for detecting active fires (in real-time). The algorithm would be developed for detecting the anomaly in brightness temperatures (Kelvin).	2.1) Is it suitable to detect forest fires on the basis of TOA brightness temperature anomalies? 2.2) What methods can be applied for detecting and extracting the fire pixels? Is it possible to develop a suitable method which would have a low error of omission and commission? 2.3) How precisely can forest fires be detected and monitored spatially and temporally with the help of MODIS, AVHRR and MSG.
3) Comparing the performance of MSG, MODIS and AVHRR in detecting forest fires. The objective is to compare the errors of commission and omission and percentage of fires detected by the 3 sensors.	3.1) What are the relative advantages and limitations of the 3 sensors when compared with each other in terms of their fire detection capabilities? How do their different characteristics namely the temporal, spatial and spectral resolutions affect their performance in fire detection? 3.2) Which is the best sensor for fire detection?

1.3 RESEARCH HYPOTHESIS

1.

H_o The MSG has relatively better capabilities for fire detection as compared with the other polar orbiting satellites MODIS and AVHRR.

H_1 The fire detection capabilities of MSG, MODIS and AVHRR are comparable.

The null hypothesis maybe reasoned as follows:
The MSG is a geostationary satellite imaging the Earth every 15 minutes and therefore, it is very useful for detecting continuously changing phenomena like active fires detection. The NOAA AVHRR and MODIS are polar orbiting with a lower temporal resolution than MSG therefore continuous monitoring of fires is not possible.
The alternative hypothesis maybe reasoned as follows:
The MSG has a coarser resolution than the polar orbiting satellites therefore the thermal response of the sensor may not be strong enough to detect fires.

2.

H_o Forest fires can be detected precisely on the basis of Top of Atmosphere brightness temperature anomalies.

H_1 The Top of Atmosphere brightness temperature anomalies cannot be used to detect forest fires precisely.

The null hypothesis maybe reasoned as follows:
Forest fires lead to high anomalies in Top of Atmosphere brightness temperatures and it is possible to locate the fires. The objective is not to know the real temperatures of the fire locations but to detect forest fires therefore atmospheric corrections are not necessary.
The alternative hypothesis maybe reasoned as follows:
The Top of Atmosphere brightness temperature anomalies might be caused due to clouds, highly reflective soils or other activities of Man. The atmospheric effects might lead to attenuation and shifts in thermal response and this may make it difficult to detect forest fires.

1.4 RESEARCH ASSUMPTIONS

- A pixel is a false alarm if it is flagged as a fire pixel for less than 3 consecutive MSG overpasses.
- After conversion of all sensor data to TOA temperatures it is possible to compare their performance without further atmospheric corrections as 2 sensors are low Earth (approx 800 km) orbiting and one is geostationary positioned (36,000 km).

1.5 RESEARCH STAGES

The research followed the following phases during the 6 months of the research period.

The first phase included reading relevant literature on the previous research which has been done in fire detection and mapping and other relevant literature pertaining to the topic. This phase also included framing my research questions, objectives and hypothesis. It was also a preparatory phase to prepare myself for fieldwork. Images were acquired and pre-processed.

The second phase included field work. A field work was done for a 3 week period in the 2 districts of Portugal (Santarem and Leiria). Data was collected from municipal organizations, forest departments, fire management organizations and personal field site observations were also conducted.

The third phase included developing a method for fire detection. Validation and analysis of my results, answering my research questions and drawing the conclusions.

2. LITERATURE REVIEW

The literature review in the following sections would focus on the spectral regions useful for fire detection, and the useful channels in the 3 selected satellites sensors for fire detection. The characteristics of the different satellite sensors in terms of their spatial, spectral and temporal characteristics vital for fire detection are also discussed. An overview of the different algorithms used for fire detection by the 3 selected satellite sensors of this study is also elaborated.

2.1 USEFUL SPECTRAL REGIONS FOR FIRE DETECTION

The electromagnetic radiation covers a wide range from the ultraviolet spectrum (short wave) to the infrared (long wave). The bands in the infrared part of spectrum are particularly suitable for fire detection and monitoring. The mid-infrared part of the spectrum produces a very strong signal during high temperatures and this makes it most suitable for fire detection. This can be explained with the help of Wien's displacement law which states an inverse relationship between the temperature of a black body and wavelength at which it has its peak emission. According to the Wien's displacement law the hotter a surface is, the peak of its temperature curve shifts to the shorter wavelengths, and the colder a surface is, its peak temperature shifts to the longer wavelengths. Wien's displacement law maybe expressed as

$$\lambda_{\max} = \frac{2898}{T}$$

Where λ_{max} is the wavelength at which the radiation is maximum, and it is expressed in µm, T is the absolute temperature in degrees Kelvin (^{o}C + 273), and 2898 is the Wien's displacement constant expressed in µm. With the help of the Wien's displacement formula it is possible to know the wavelength at which the radiation peaks if the temperature of the blackbody is known (Kerle et al., 2004). For example when the temperature is 750 K (fire condition) them on applying Wien's displacement law the maximum temperature would be along band 3.9 micron. But, if the temperature is 300 K (normal non-fire condition) the maximum temperature would be at band 9.7 micron.

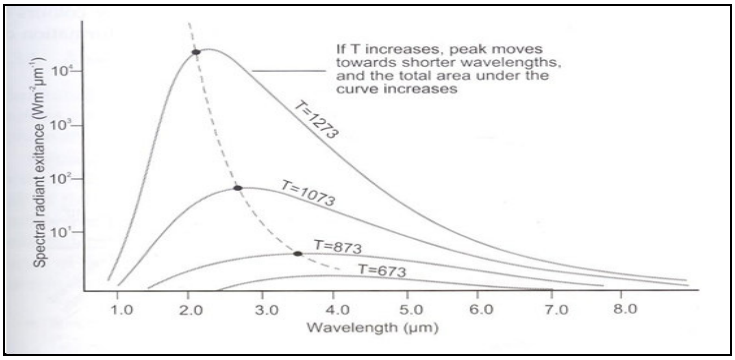

Figure 2. 1 Blackbody radiation curves. *Source (Kerle et al., 2004)*

Figure 2.1 depicts the different Blackbody radiation curves as expressed by Wien's displacement law.

Another important consideration in fire detection is the position of the bands with respect to the atmospheric transmissions. The bands located along CO2 absorption (λ_{cen} 13.40 micron), water vapour absorption (λ_{cen} 7.05 micron) and O_3 absorption (λ_{cen} 9.580 micron) have lower brightness temperatures due to absorption and low transmission of energy. The atmospheric windows are the portions of the spectrum having little atmospheric absorption and high transmission of energy. In the thermal infrared region these are located between 3-5 micron, and 8-12 micron, these bands are useful for fire detection (Kerle et al., 2004).

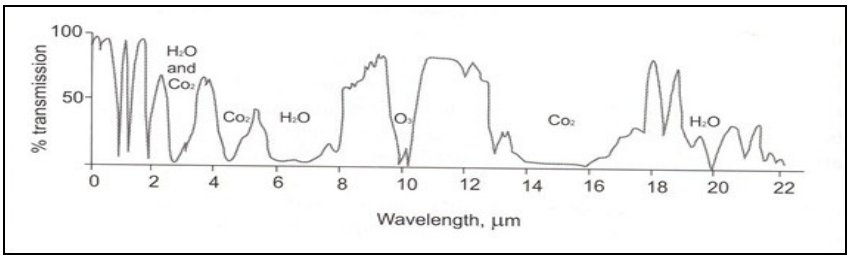

Figure 2. 2 Atmospheric transmissions. *Source (Kerle et al., 2004)*

2.1.1 Response of 3.9 μm and 10.8 μm to sub-pixel hotspots

Most of the fire detection studies have used band 3.9 λ_{cen} and 10.8 λ_{cen} micron for detection of fires. This section therefore makes a comparison of these 2 bands.

a) Effect of solar reflection and earth's radiant energy

Figure 2.3 shows that the 3.9 micron band during the day receives reflected energy from the sun and the Earth's radiant energy; however, during the night it receives only the Earth's radiant energy. Therefore, this band responds differently to hotspots at day and night. 10.8 micron band receives only the Earth's radiant energy during the day and night and therefore it differs in hotspot response as compared to 3.9 micron band (EUMETSAT; and CGMS, 1999).

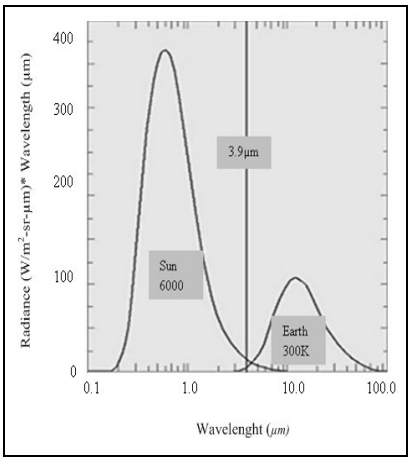

Figure 2.3 Effect of solar radiation on 3.9μm

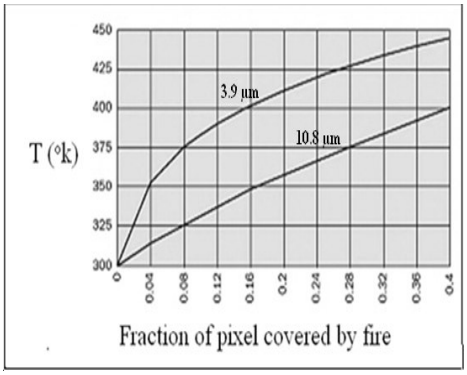

Figure 2.4 Response of 3.9 &10.8μm to fraction of pixel covered by fire

Source (EUMETSAT; and CGMS, 1999).

b) Response of 3.9 μm and 10.8 μm to sub-pixel hotspots

Figure 2.4 shows the response of 3.9 μm and 10.8 μm to sub-pixel fires. The temperature of band 3.9 μm is 350^{o} K when the fire occupies 4% of the pixel, and remains substantially higher as the area of the hotspot in the pixel increases. The temperature of band 10.8 μm is 35^{o} K lower than band 3.9 μm when the fraction of pixel covered by fire is 4% (EUMETSAT; and CGMS, 1999).

The 3.9 μm has a strong thermal response even if only a small portion of the pixel is covered by fire and this characteristic is vital for fire detection and this would help in the selection of useful channels in MSG, MODIS and NOAA AVHRR for this research.

2.2 CHARACTERISTICS OF THE 3 SATELLITE SENSORS

Broadly with respect to the overpasses and orbital characteristics satellites maybe broadly divided into geostationary satellites and polar orbiting satellites. Geostationary satellites are very useful to map active fires. Since they have a high temporal resolution they give very important information about phenomena which change continuously. The polar orbiting satellites have a higher spatial resolution since they have a lower orbital altitude and this characteristic makes them important for several studies. The polar orbiting satellites have another advantage over the MSG; they include larger areas of the earth than the MSG. However, it would be really useful to combine both the benefits of the geostationary satellites and polar orbiting satellites by combining their strengths.

2.2.1 Characteristics of MSG

a) General information

The first European geostationary Meteosat satellites were launched in 1977. The Meteosat first generation series got replaced by the Meteosat Second Generation (MSG) after the launch of MSG in August, 2002. It is established under cooperation between the European Space Agency (ESA) and the European Organization for the Exploitation of Meteorological Satellites (EUMETSAT). The MSG consists of 4 geostationary meteorological satellites that would remain operative untill 2018. The MSG continuously images the full disk of the earth with the help of the Visible and Infrared Imager (SEVIRI) imaging radiometer. Along with the SEVIRI the MSG satellites carries the GERB (Geostationary Earth Radiation Budget) instrument which provides data on the reflected solar radiation and thermal radiation emitted by the Earth and its atmosphere. The calibration of the infrared bands is carried onboard in SEVERI and the accuracy is 1K for thermal IR channels. MSG has a geostationary orbit at an altitude of 35,600km over the Earth.

b) Temporal resolution

The SEVIRI images the earth in a wide spectral range in 12 channels, at an interval of 15 minutes. For channels 1-11, a full disk image consists of 3712 * 3712 pixels, however for the HRV channel a complete image consists of 11 136 * 5568 pixels and it covers only half-disk in a East-West direction.

c) Spatial resolution and spatial coverage

3km at sub-satellite point (11 bands) and HRV band has a spatial sampling distance of 1km. The instantaneous field of view of the channels is about 4.8 and 1.67 km and since the detectors are diamond shaped the views are oriented at an angle of 45^{o},

therefore the subtended angle remains constant for each pixel and the spatial resolution of the pixel decreases as the distance increases from nadir, which in case of MSG is the Equator (Schmetz et al., 2002) and (www.eumetsat.int). For more detail information on MSG, its characteristics and functions the given references maybe referred.

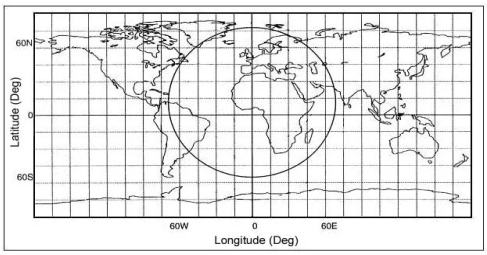

Figure 2.5 MSG spatial coverage. *Source: http://www.eumetsat.int*

d) Spectral characteristics

Table 2.1: Spectral characteristic of MSG SEVERI channels.

Channel	Band	Wavelength range ($\lambda_{min} - \lambda_{max}$)	Centre wavelength (λ_{cen})	Main gaseous absorber or window
1	VIS 0.6	0.56 - 0.71	0.635	Window
2	VIS 0.8	0.74 - 0.88	0.81	Window
3	IR 1.6	1.50 - 1.78	1.64	Window
4	IR 3.9	3.48 - 4.36	3.92	Window
5	WV 6.2	5.35 - 7.15	6.25	Water vapour
6	WV 7.3	6.85 - 7.85	7.35	Water vapour
7	IR 8.7	8.30 - 9.10	8.7	Window
8	IR 9.7	9.38 - 9.94	9.66	Ozone
9	IR 10.8	9.80 - 11.80	10.8	Window
10	IR 12.0	11.00 -13.00	12	Window
11	IR 13.4	12.40 - 14.40	13.4	Carbon dioxide
12	HRV	0.4 - 1.1	0.75	Window/ water vapour

Source: (Schmetz et al., 2002) and (www.eumetsat.int)

2.2.2 Characteristics of NOAA AVHRR

a) General information

The AVHRR is jointly managed by The National Oceanic and Atmospheric Administration (NOAA) and the National Aeronautics and Space Administration (NASA). The first NOAA satellites the TIROS-N, was launched in October 1978,

after which a series of NOAA satellites were launched. AVHRR is a scanning radiometer on the satellite. The first AVHRR carried on TIROS-N (1978) was 4-channel radiometer, AVHRR/2 was improved to 5 channels and presently, AVHRR/3 is a channel 6 instrument carried in NOAA-15 (launched in 1998). The sensor has a sun-synchronous orbit at 833 km and orbits the earth 14 times daily.

b) Temporal resolution

The NOAA AVHRR/3 radiometer images a place 2 times in 24 hours. However, since AVHRR/3 is carried on 3 NOAA satellites (NOAA-15, 16, 17 and 18) therefore a location may receive more images if the images of all the operational satellites are combined.

***c)* Spatial resolution and spatial coverage**

The AVHRR has a swath width measuring 2400 Km, and a spatial resolution of 1.1km at sub-satellite pixel.

d) Spectral characteristics

5 channels transmit data at a time, since channel 3A and 3B cannot operate at the same time. Further information on AVHRR/3 maybe acquired from the KLM user guide, September 2000 version (Goodrum et al., 2000).

Table 2.2: Spectral characteristic of AVHRR/3

BANDS	BAND RANGE ($\lambda_{min} - \lambda_{max}$)	IFOV MILLIRADIANS	APPLICATIONS
1	0.58 - 0.68	1.39	Cloud and snow monitoring
2	0.725 - 1.10	1.39	Water and agricultural studies
3A	1.58 to 1.64	1.39	Detection of change in albedo level
3b	3.55 to 3.93	1.39	Cloud mapping, sea surface temperature
4	10.50 - 11.50	1.39	Cloud mapping, sea surface temperature
5	11.5 - 12.5	1.39	Sea surface temperature

Source: (Goodrum et al., 2000)

2.2.3 Characteristics of MODIS

a) General information

The Moderate Resolution Imaging Spectroradiometer (MODIS) is on-board the Terra and Aqua satellites. Terra is managed by 'NASA's Goddard Space Flight Centre' and is multi-national, multi-disciplinary mission involving many partners. The Aqua is an integral part of the 'Earth Observing System (EOS)' which is centred at NASA. Terra overpasses the Earth in the morning from North towards South

across the Equator, and Aqua overpasses the earth in the afternoon but from south to North across the equator and flies at a height of 705km.

b) Temporal resolution

MODIS images a given place 4 times in 24 hours, recording 2 images at day and 2 images at night.

c) Spatial resolution and spatial coverage

MODIS has a swath width of 2330 km cross track and 10km along track which leads to a maximum scan angle of 55^{o} at both ends of the flight line. Therefore, the instantaneous field of view increases from 1x1 km at nadir to about 2x5 km at the maximum scan angle. At the edge of the image this causes a repetition of features which is referred to as Bowtie-Effect and therefore proper geometric corrections are necessary (Wolfe; et al., 2002). Refer to Table 2.3 for spatial resolution

d) Spectral characteristics

Table 2.3: Spectral characteristic of MODIS

BAND NUMBER	BAND RANGE	SPATIAL RESOLUTION M	BAND NUMBER	BAND RANGE	SPATIAL RESOLUTION (M)
1	620 - 670	250	19	915 - 965	1000
2	841 - 876	250	20	3.660 - 3.840	1000
3	459 - 479	500	21	3.929 - 3.989	1000
4	545 - 565	500	22	3.929 - 3.989	1000
5	1230 - 1250	500	23	4.020 - 4.080	1000
6	1628 - 1652	500	24	4.433 - 4.498	1000
7	2105 - 2155	500	25	4.482 - 4.549	1000
8	405 - 420	1000	26	1.360 - 1.390	1000
9	438 - 448	1000	27	6.535 - 6.895	1000
10	483 - 493	1000	28	7.175 - 7.475	1000
11	526 - 536	1000	29	8.400 - 8.700	1000
12	546 - 556	1000	30	9.580 - 9.880	1000
13	662 - 672	1000	31	10.780 - 11.280	1000
14	673 - 683	1000	32	11.770 - 12.270	1000
15	743 - 753	1000	33	13.185 - 13.485	1000
16	862 - 877	1000	34	13.485 - 13.785	1000
17	890 - 920	1000	35	13.785 - 14.085	1000
18	931 - 941	1000	36	14.085 - 14.385	1000

Source: modis.gsfc.nasa.gov (Bands 1 to 19 are in nm; Bands 20 to 36 are in µm)

Table 2.3 gives an overview of the spectral characteristics of MODIS. Further information and details about the technicalities and uses of MODIS maybe acquired from the MODIS homepage at http://modis.gsfc.nasa.gov/about/media.php

Influence of solar zenith angle and scan angle on fire detection: The solar zenith angle and the scan angle are 2 very important influences on the thermal anomaly detected by a sensor. All other conditions remaining constant a fire would be prominent as compared to its background at a larger solar zenith angle than at a smaller solar zenith angle. At smaller solar zenith angles the influence of solar radiation is very high and therefore the 3.9 temperature is raised. With increasing scan angle the pixel area increases and therefore the apparent brightness temperature decreases for the pixels. Comparing this effect for 3.9 µm and 10.8 µm it is seen that the temperature decrease is more for 3.9 µm. The decrease is mainly noticed for small fires (<100 ha) however incase of large fires (>100 ha) the temperature of 3.9 µm remains the same and that of 10.8 decreases. An added cause for the decrease in brightness temperature due to scan angle increase is the increase in atmospheric absorption (GIGLIO.; et al., 1999).

2.3 REVIEW OF FIRE DETECTION ALGORITHMS

The following sections give a brief review of research which has been done in detection of forest fires using NOAA-AVHRR, MODIS and MSG SEVIRI. The review focuses on studies which have used thermal bands to detect fire, on the basis of a thermal anomaly of Top of atmosphere (TOA) brightness temperatures. It will give a brief outline on the method of extraction of fire pixels, the limitations of the method and further suggestions. The review is in 3 main sections each focusing on MODIS, AVHRR and MSG SEVERI satellite sensors.

2.3.1 MSG

Not many fire detection algorithms have been developed for fire detection with MSG SEVERI satellite sensor. (AYANZI et al., 2005) in their study have used the 3.9 µm and 10.8 µm for fire detection. The authors used the contextual method for detection where for N x N spatial matrix of pixels. The mean and standard deviation of the matrix for the 2 bands were calculated and fire was detected based on the following algorithm.

$$T_{3.9\mu m} > \mu_{3.9\mu m} + f.\sigma_{3.9\mu m}$$
$$T_{3.9\mu m} - T_{10.8\mu m} > \mu_{dif} + f.\sigma_{dif}$$

The algorithm states that T (temperature ^{o} K) for a pixel at 3.9 µm should be more than the mean (µ) + standard deviation (f.σ) of 3.9 µm of the selected N x N pixels. The second condition was that the difference between T (temperature ^{o} K) for a pixel

at 3.9 µm and 10.8 µm should be more than the mean difference of 3.9 µm and 10.8 µm + standard deviation of 3.9 µm and 10.8 µm of the N x N pixels. The fire pixels were validated with MODIS images. The authors claim that they have noticed a large number of false alarms in their method of fire detection.

(Van Den Bergh and Frost, 2005) used another approach for detection where they built a model of the normal diurnal cycle of the area. The mean and standard deviations of each of the 96 images of the day were computed. They claimed that slope of the diurnal cycle would be the same even if the absolute temperatures were not same for a homogeneous area. The results of the model were used in a Kalman filter model which used the previously observed data to predict the expected temperature for a pixel. The predicted value is then compared with the observed value of the pixel, a threshold was applied to the difference in observed and predicted value which indicated whether there was a fire or not. The research was validated with the MODIS fire products. There were number of pixels flagged fire pixels which were not in the MODIS product, however, these could be false alarms. Many fires were not flagged which were flagged in the MODIS product, and the authors blamed the spatial resolution of MSG to be the cause. There were no ground truths for validation and the algorithm was applied to a small area over a short range of days. Therefore, it is very difficult to draw a conclusion about the quality of this procedure. There are no MSG SEVIRI fire products till today but since January 2007 a few fire products were on the EUMETSAT website on a trial basis. There is no information on the procedure they applied for detecting fires. (www.eumetsat.int)

2.3.2 MODIS

Kaufman et al (1998) in their paper has described the algorithms they used for fire detection. They have placed different thresholds for night and day fires, since during night the 3.9 µm has a lower signal since there is no sunlight reflection. The pixels for which the temperature of 3.9 µm was less than 315K (day) or 305K (night) or the temperature difference between 3.9 µm and 10.8 µm was less than 5K (day) and 3K (night) were considered as non-fire pixels. They derived fire detection methods involving absolute temperature and relative temperature. In absolute fire detection method, a pixel to be considered as a fire pixel had to be more than 320K (day) and 315K (night) and the difference between the temperature at 3.9 µm and at 10.8 µm must be more than 20K (day) and 10K (night). But if the temperatures were more than 360K (day) and 330K (night) then the threshold for difference between the temperature at 3.9 µm and at 10.8 µm is not applied. In relative fire detection, the fire pixels are detected on the basis of the channel 3.9 µm and 10.8 µm, the difference between the standard deviations of pixel at 3.9 µm and standard deviation

of pixel at 10.8 µm should be at least 2K. The MODIS cloud mask product was used to detect fires during cloud conditions and the algorithm was applied only for the non-cloud conditions. The algorithm however had some limitations, small fires many times remained unnoticed and there were a number of false alarms in deserts and areas which had sparse vegetation.

Therefore Giglio et al (2003) improved some aspects of the MODIS original algorithm. Their algorithm used channel 4 (3.9 µm) and channel 11 (10.8 µm) denoted by T4 and T11 channels. Channel 21 and 22 at 3.9 µm saturates at 500 K and 331 K respectively. Therefore, T4 is derived from channel 22 since it has a lower saturation and therefore less noisy. T11 is derived from channel 31 (10.8 µm) with saturation level of 400K (Terra MODIS) and 340K (Aqua MODIS). Channel 32 (12 µm) is used for cloud masking; Channel 7 (2.13 µm) is used to remove false alarms generated due to water. Daytime pixels are considered to be cloud-obscured if the following condition is satisfied:

The reflection of channel 1 (0.65 µm) plus channel 2 (0.86 µm) must be higher than 0.9 or channel 32 (12 µm) must have a temperature less than 265K, or reflection of channel 1 (0.65 µm) plus channel 2 (0.86 µm) must be higher than 0.7 and channel 32 (12 µm) must have a temperature more than 285K.

$$(P_{0.65} + P_{0.86} > 0.9) \text{ or } (T_{12} < 265K) \text{ or}$$
$$(P_{0.65} + P_{0.86} > 0.7) \text{ and } (T_{12} < 285K)$$

During the night it just has to fulfill the condition that temperature of channel 32 is less than 265 K to be called a cloud obscured pixel (T12 < 265 K). The image is classified into different classes (*missing data, cloud, water, non-fire, fire, or unknown)*, the fire detection task then continues with the remaining land pixels. The fire detection algorithms which they used maybe classified as 2 types, absolute threshold or relative threshold method. An absolute threshold test is conducted where a pixel should have the following characteristic to be considered a fire pixel.

$$T_4 > 330K (320K \text{ at night}) \text{ or}$$
$$T_4 > 330K (315K \text{ at night}) \text{ and } T_4 - T_{11} > 25K \text{ (10K at night)}$$

An algorithm is then applied for relative fire detection, by which is meant the fire pixels are extracted by comparing their brightness temperatures with the surrounding pixels. Combining the different algorithms a pixel is flagged as fire if the following conditions are satisfied:

$$T_4 > mean(T_4) + 3stddev(T_4) \text{ or } T_4 > 330K \text{ (day)}$$
$$T_4 > mean(T_4) + 3stddev(T_4) \text{ or } T_4 > 315K \text{ (night)}$$

AND

$$T_4 - T_{11} > median(T_4 - T_{11}) + 3stddev(T_4 - T_{11}) \text{ or } T_4 - T_{11} > 25K \text{ (day)}$$
$$T_4 - T_{11} > median(T_4 - T_{11}) + 3stddev(T_4 - T_{11}) \text{ or } T_4 - T_{11} > 10K \text{ (night)}$$

Apart from this the paper introduces a number of algorithms which maybe used for particular regions to remove special effects like the desert boundary effects, coastal false alarm rejection algorithm (Giglio et al., 2003)

2.3.3 AVHRR

AVHRR has been used for fire mapping since 1980 some of the AVHRR results have been used for preparing and designing MODIS products, for instance The Joint Research Center of Italy and ESA-ESRIN used AVHRR results for making fire distributions products over Africa, a second example being the operational real-time detection program of INPE, Brazil. AVHRR first fire detection applications were on targets which had a known and fixed location. Matson and Dozier in 1981 studied the gas flares from oil fields in the Middle East and steel mills in the Midwestern United States, with the help of 3rd-generation NOAA-6 satellite. Following the fixed locations fire detections the AVHRR was used for fire detection (Kaufman et al., 1998). Some important works which have developed algorithms for fire detection maybe as follows:

Li et al (2000), in their paper proposed algorithms for fire detection based on thresholding which consisted of marking the potential fires and also removing the false alarms. A brightness temperature of channel 3b (3.9 μm) $T_3 = 315K$ was chosen for detecting the possible fire pixels. This threshold led inclusion of most of the fires but also many false alarms. It was necessary to remove the alarms; therefore 3 thresholds were applied to the possible fire pixels to remove the false alarm pixels. According to the first threshold the difference between channel 3b (3.9 μm) and channel 4 (11 μm) brightness temperatures must be more than or equal to 14K to be considered as fires $T_3 - T_4 \le 14K$, the rest are eliminated as false pixels. The next threshold uses channel 4 (11 μm) to delete the signal from highly reflective clouds; it removes the pixels which are below 260K as possible fires and pixels more than 260K are flagged as fires ($T_4 > 260K$). The next threshold intended to remove false alarms from the surface and considered pixels with *R*eflectance (R_2) more than 0.22 in channel 2 (0.7 μm) as false alarm pixels. Another thresholding was done to remove the effect of clouds, where the difference between channel 4 at 11 μm (T_4) and channel 5 at 12 μm (T_5) is $T_4 - T_5 \ge 4.1K$ and difference between channel 3b at 3.9 μm (T_3) and channel 4 at 11 μm (T_4) is $T_3 - T_4 < 19K$ those pixels are removed as false fires. There were then 2 screening performed so as to remove false alarms. The first removes all non-forest pixels and the second removed all single hotspot pixels since all Boreal forest fires were more than 1km.

Arino and Melinotte (1998) detected possible fires with the help of AVHRR channel 3b at 3.9 μm which detected possible fires around 320K. A number of thresholds were then applied for removing the false alarms. The first test demanded that the brightness temperature of channel 3b (3.9 μm) must be greater than channel 4 (11 μm) by 15K. The second test removed the effect of clouds and demanded that the brightness temperature must be more than 245K to be considered as fire. In the next test pixels with a reflection of more than 0.25 were excluded as false alarms. To remove the false alarm due to glitter the next test required the difference between channel 1 (0.5 μm) and channel 2 (0.7 μm) reflectance to be more than 0.01. The next test was applying a quick look (QL) inspection to check the quality of the detection. In the next step a vegetation mask is applied and fires are compared with NDVI.

Giglo et al (1999) criticized the Arino et al (1993) threshold as being too high for certain areas in the world like the tropical rainforest, temperate deciduous forest and boreal deciduous forest where the temperatures for small fires (100m2) are usually lie between 308 and 314K. He maintained that fires which were cooler and smaller would not be detected well by Arino et al (1993) threshold methods. He came up with results that in the boreal forest 60% of the fires had a temperature below 320K and this number of 70% in tropical rain forest, and 85% in the savanna. Therefore, the thresholds could not be applied on a big scale and could be applied in a regional scale. The authors in this paper therefore presented an alternative algorithm. A pixel is flagged as a potential fire pixel if the following conditions are fulfilled

$$T_3 > 310K, T_3 - T_4 > 6K, \text{and } r^2 < 0.25 \text{ (Day)}$$

$$T3 > 308K \text{ and } T3\ 4 > 4K \text{ (night)}$$

T_3 is temperature for 3.9 μm and T_4 is temperature for 11 μm; r^2 is reflectance for 0.5 μm. His main objective was to view more of the smaller fires. He applied this algorithm on the same images used by Arino et al (1993) and his method detected more fires, especially in case of savanna, where there was 35% increase in the number of fires detected.

The IGBP fire detection method performed in 2 stages. The first stage is called the threshold test where a pixel is considered to be a fire if the brightness temperature (T_B) of channel 3b (3.9 μm) is more than 311K; and the brightness temperature (T_B) of channel 3b (3.9 μm) minus channel 4 (11 μm) to be greater than 8K

$$T_B(3) > 311K$$
$$T_B(3) - T_B(4) > 8 \deg K$$

The second stage is to apply another test to these potential fire pixels selected from the above threshold test, the main aim of this stage is to remove the pixels which are

affected a lot of reflection. The pixels for which channel 2 is above 20% are removed as potential fires.

$$Ch\ (2) < 20\%$$

In the next stage a pixel is flagged as fire if it fulfils the following conditions

$$[T_B(3) - T_B(4)] > \max\{T_B(34)bg + \sigma(34)bg, 3K\}$$

$$T_B(3) > T_B(3)bg + 2\sigma(3)bg + 3K$$

Where T_B is the brightness temperature, max is maximum, $TB(34)bg$ Is the mean value difference between channel 3 and 4, $\sigma(34)bg$ is the standard deviation difference of channel 3 and 4, $TB(34)bg$ is the mean of channel 3 (3.9 μm), σ is the standard deviation (Stroppiana.; et al., 2000).

Kaufman et al (1995) evaluated the performances of the Canada Centre for Remote Sensing (CCRS) algorithm developed by Li et al (2000); the European Space Agency (ESA) algorithm developed by (Arino et al. 1993); the algorithm of Giglo et al (1999); the Project (IGBP) Algorithm developed by Justice et al. 1993, 1996, Justice and Dowty 1994, Flasse and Ceccato 1996 and the operational MODIS algorithm developed by Kaufman et al. 1998 and they came up with the following comments.

Table 2.4: Performance of the algorithms

	CCRS	ESA	GIGLIO ET AL	IGBP	KAUFMAN
Omission error	46%	81%	75%	51%	81%
Commission error	30%	21%	59%	50%	22%

Source: (Kaufman et al., 1998)

The IGBP algorithm has been applied globally; the ESA algorithm was only used in the tropics. The Giglio algorithm has yet not been applied globally. The CCRS algorithm is designed for Canadian boreal forests. Therefore, the CCRS performed best since it was validated with boreal forest fires. The IGBP flagged the largest number of pixels as fire pixels, followed by CCRS and GIGLIO algorithms which were close to each other in the number of pixels they flagged, followed by the ESA and MODIS flagged pixels.

2.4 SUMMARY

This chapter discusses the spectral regions which are important for fire detection.

The literature review reveals that the 3.9 µm is the best region for fire detection along with the 10.8 µm. The 3.9 µm and 10.8 µm are compared on their capabilities for fire detection; the 3.9 µm appeared superior in its capabilities for fire detection. The next section discusses the spectral, spatial and temporal characteristics of MODIS, MSG SEVIRI and NOAA AVHRR. The following section gives a review of the different algorithms developed for detecting fires with MODIS, MSG and NOAA AVHRR. The review of the algorithms revealed that there is no global algorithm which can be used for all climates and regions. Every algorithm faced errors of commission and omission; if the errors of omission were lower it was balanced by a higher error of commission and vice versa. On comparing the algorithms developed for the 3 sensors it is revealed that a number of algorithms have been developed and validated for MODIS and AVHRR, though the performance of them is questionable. But, in the case of MSG there are not many algorithms developed and the further none have been validated for global commercial products.

3 MATERIALS AND METHODS

3.1 STUDY AREA

The study area of this research work includes 2 districts in central Portugal, Leiria and Santarem which have a Mediterranean climate with hot dry summers and cool wet winters. Fires mainly occur during the summer months when the high temperatures followed by low rainfall and accompanied drought conditions trigger forest fires. Santarem is located in central Portugal on the right bank of the Tagus River. It has an area of 560 km^2. The geographic coordinates of Santarem is 39^{o}12'N and 8^{o}42'W (Wikipedia 2006a). Leiria is located on the west coast of Portugal at 39^o 46'N and 8^o 53' W, it has an area of 565 km^2 (Wikipedia 2006b). The regions having higher altitudes are covered more with vegetation than the flatter and lower areas. Therefore, the areas with a higher altitude have a larger incidence of forest fires in Portugal. Figure 3.1 shows the study area in Portugal and the altitude of areas within the study area.

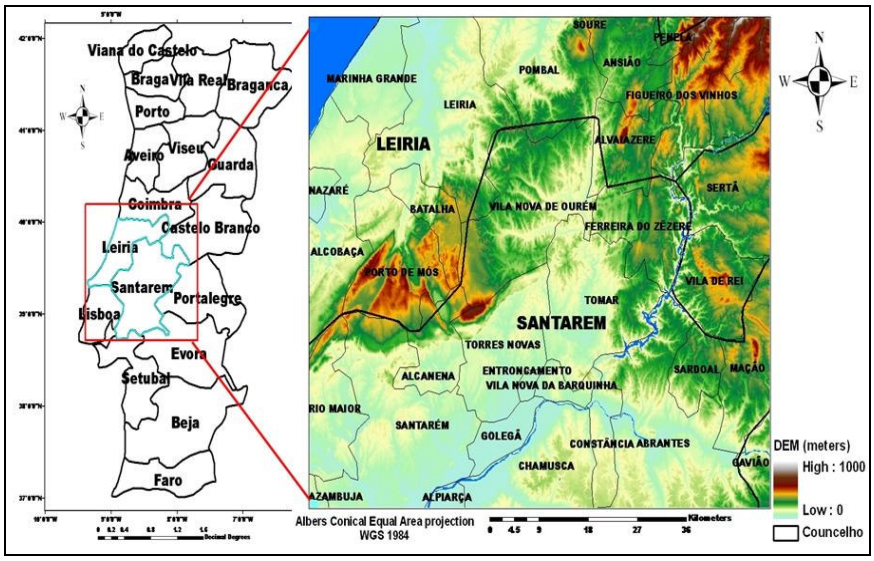

Figure 3.1 The study area in Portugal

3.1.1 Fires in Portugal

The forests of Portugal are continuously plagued with forest fires. There are a number of reasons for frequent occurrence of fires. As observed during field work it

was seen that agricultural practices are traditional and farmers burn the vegetation to prepare the soil for crops. Fire is also resorted to for removing unwanted vegetation and waste. There have been a number of incidences when people have been careless with fire on fire alert days in the country. For example the fire caused in Penhacosa in Macao on 4th august 2006 was caused by a man cutting iron rods in the forest on a red alert day, the sparks led to a fire which destroyed 244.47 hectares of forest. There are also a small number of groups with political motives which deliberately set forest on fire. The forest species in Portugal are fire prone; examples of species include the eucalyptus, pine and cork oak. Meteorological conditions also favour forest fires in Portugal. Figure 3.2 shows the causes in Portugal in 2006.

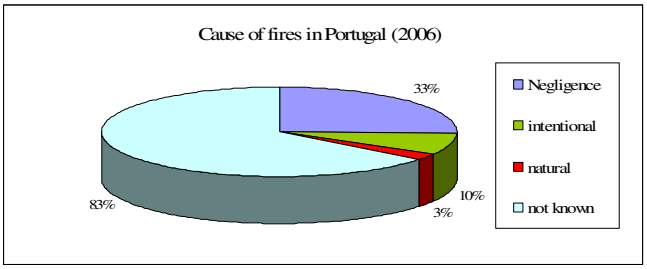

Figure 3.2 Cause of forest fires in Portugal (2006) *Source DGRF (2006)*

The number of fires has increased in Portugal over the last 2 decades. The average number of fires in 1980-1989 was 6777, during 1990-1999 it was 22250, and in 2000 there were 34109 fires. The average burnt area in the year 2000 was 159604 (ha), between 1980 and 1990 was 74 500 ha, and in 1990-1999 was 102 203 ha (European Commission, 2001). In 2005 there was intensive drought, which led to the largest number of fires since 1980, which was the first year of data collection. There were 35698 fires and the total burnt area was 338262 ha. By August 2005, 71 % of Portugal was classified as being in extremely drought conditions and 29 % severe drought conditions which led to a large number of fires (European Commission, 2006b). In 2004 there were 21,891 fires which burnt a total area of 129652 hectares. In June and July the rising temperatures and strong winds led to massive fires. 50,600 ha were burnt in July and 60,677 ha in June (European Commission, 2005). Since the last 23 years the worst fire records was in 2003. There were 20864 fires which burnt an area of 421835. 66% of the fires took place in the month of August when high temperatures, low humidity and lighting triggered a number of fires (European Commission, 2004). In 2002 the number of fires in Portugal was 26469 which burnt an area of 123910 hectares. 86% of the fires took place during the months of July and August (European Commission, 2003b and 2003a). With the help

of MODIS and the European CORINE Land Cover 2000 (CLC 2000) database the burned areas of 2006 untill September 2006 were mapped. Spain is leading with 118 401 ha of burnt area followed by Portugal with 56 453 ha of burnt areas (European Commission, 2006). Figure 3.3 shows the Number of fires and burnt area in Portugal (1980-2006). Figure 3.4 compares the monthly occurrence of fires for the different years. The largest number of fires and maximum burnt area for the different years are during July and August.

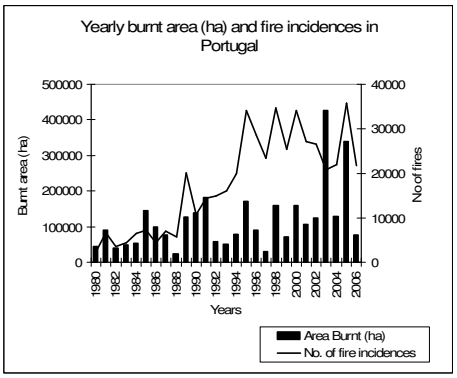

Figure 3.3 Yearly fires and burnt area.

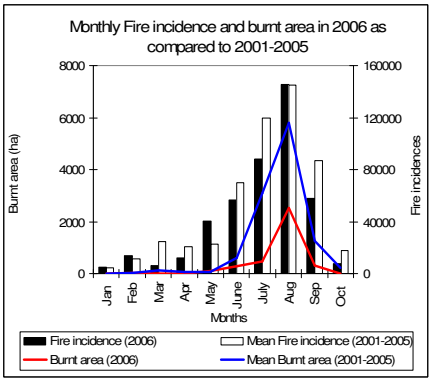

Figure 3.4 Monthly fires and burnt area

Source: (DGRF, 2006)

The districts of Santarem and Leiria have a large number of fires every year; the following table shows the burnt area from 2003-2006.

Table 3.1: Yearly burnt area in the study area

DISTRICT	2003	2004	2005	2006
Santarem	59280	5456	30673	2833
Leiria	7344	688	6026	5206

Source: (DGRF, 2006)

Weather and Occurrence of Fire in Portugal: Portugal has climatic conditions which create favourable conditions for the fires to occur. The climate of Portugal maybe broadly categorized into 2 broad zones, the northern and the southern zones. The northern zone is influenced by the Spanish Meseta and the Siberian anticyclones which make it comparatively cooler than the South. The temperatures in the northern zone are 4–9^{o}C in the winter and 21^{o}C summer. The southern zone is influenced by the Azores high-pressure system which make the summer months hot and dry in the South. The temperatures in the southern zone may rise to 35-40^{o}C in summer and 10^{o} C in winter (Britannica, 2006 and Wikipedia 2006). The institute of Meteorology

since 2002 has used the Canadian system of *'Forest Fire Weather Index' (FWI)* to calculate the fire risks each day for Portugal. The parameters which are considered for calculating the Fire risk are the temperature of the air, relative humidity, wind speed and precipitation during the last 24 hours. The FWI consists of 6 components which maybe divided into 2 categories: The fuel moisture codes and fire behaviour indexes. The fuel moisture codes consists of *'Fine Fuel Moisture Code (FFMC)'* which rates the moisture content of very fine litter since this governs the flammability of the litter, '*Duff Moisture Code (DMC)'* rates the moisture content of medium size litter and litter at moderate depth *and 'The Drought Code (DC)'* rates the moisture content of the organic matter which is very deep and compact. The 3 codes use weather observations to calculate the codes. The FFMC uses temperature, relative humidity, wind and rain; the DMC uses temperature, relative humidity, and rain; and DC uses the temperature and rain. The fire behaviour indexes are the *'Initial Spread Index (ISI)',* calculates the rate at which the fire is expected to spread, the *'Buildup Index (BUI)'* calculates the total amount of fuel which is available for burning and the *'Fire Weather Index (FWI)*'rates the fire intensity. The ISI is calculated with the help of FFMC and wind, the BUI is calculated with the help DMC and DC, and FWI is combines the BUI and ISI. Therefore, in short the FWI is made up of different components which are calculated with weather data: temperature, rainfall, wind speed and relative humidity. The final risk is divided into 5 categories: Low alert, Moderate alert, raised alert, moderately raised alert, and high alert (Global Fire Monitoring Centre (GFMC) and Instituto De Meteorologia).

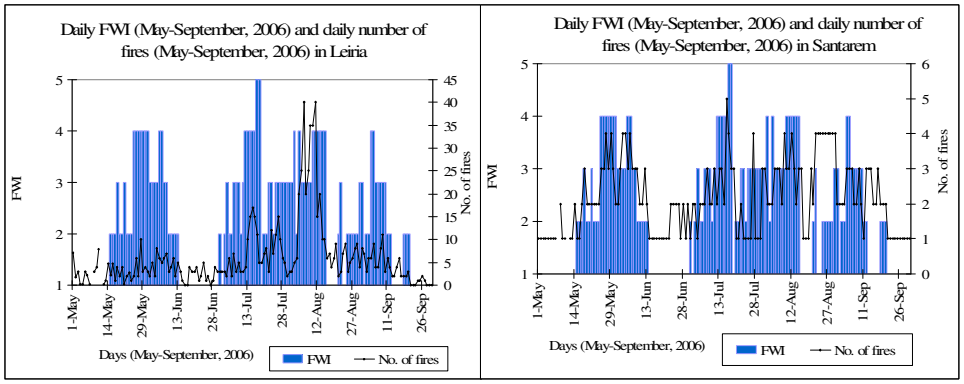

Figure 3.5 FWI and fire frequency. *Source: Instituto De Meteorologia (2006a)*

Figure 3.5 show the daily FWI (May-September, 2006) and daily number of fires (May-September, 2006) in Leiria and Santarem. FWI 1 represents Low alert, 2 being Moderate alert, 3 being raised alert, 4 being moderately raised alert, and 5 being high

alert. Fires have also occurred on no alert days therefore, it seems that Man also has a role to play in the occurrence of fires in these districts.

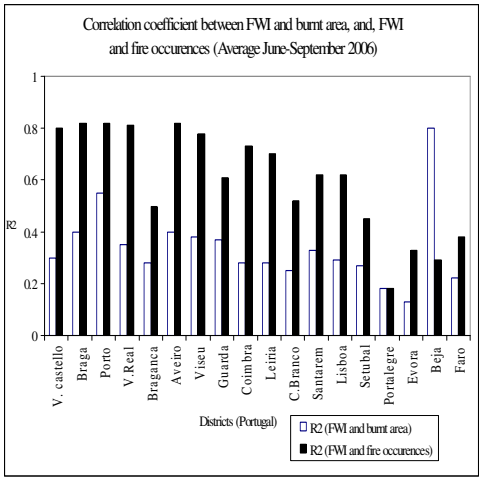

Figure 3.6 Correlation of FWI and fire

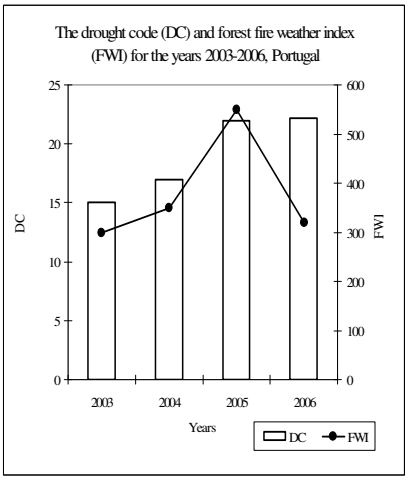

Figure 3.7 Drought index and FWI

Source: Instituto De Meteorologia (2006)

Figure 3.6 shows the average (June–September, 2006) coefficient of correlation between FWI and burnt area, and FWI and fire occurrence for the districts of Portugal. The average (June to 30 September) coefficient of correlation between the FWI and burnt area is 0.35 for Santarem and 0.3 for Leiria, with the maximum correlation being in the month of August, 0.48 (Leiria) and 0.38 (Santarem). The coefficient of correlation between the FWI and fire occurrence is 0.65 and 0.7 for Santarem and Leiria respectively, the maximum correlation is in the month of August, 0.85 (Leiria) and 0.61 (Santarem) Figure 3.7 shows the drought code (DC) and the FWI for the years 2003, 2004, 2005 and 2006. Ranking the years from 2003 to 2006, the FWI was highest in 2005 followed by 2004, 2006, 2003, and the same trend was noticed in the DC trend. It is clear from the graphs that weather conditions trigger fire, since 2005 had the maximum number of fires and it also had the highest FWI and drought

3.2 STAGES OF RESEARCH METHOD

Pre field work stage: This stage included field work preparation including sampling design for field work and preparation of the images and maps which would be used for guidance during field. The images which would be used for fire detection were also pre-processing, which included geometric correction, converting DN values to radiance and further to temperature values (K).

Field work stage: Data collection in field study area.

Post field work stage: This stage include selection of appropriate bands for the research and detection of thermal anomaly; developing, testing and refining the fire detection algorithm, validation and analysis of the research. Figure 3.8 outlines the research approach

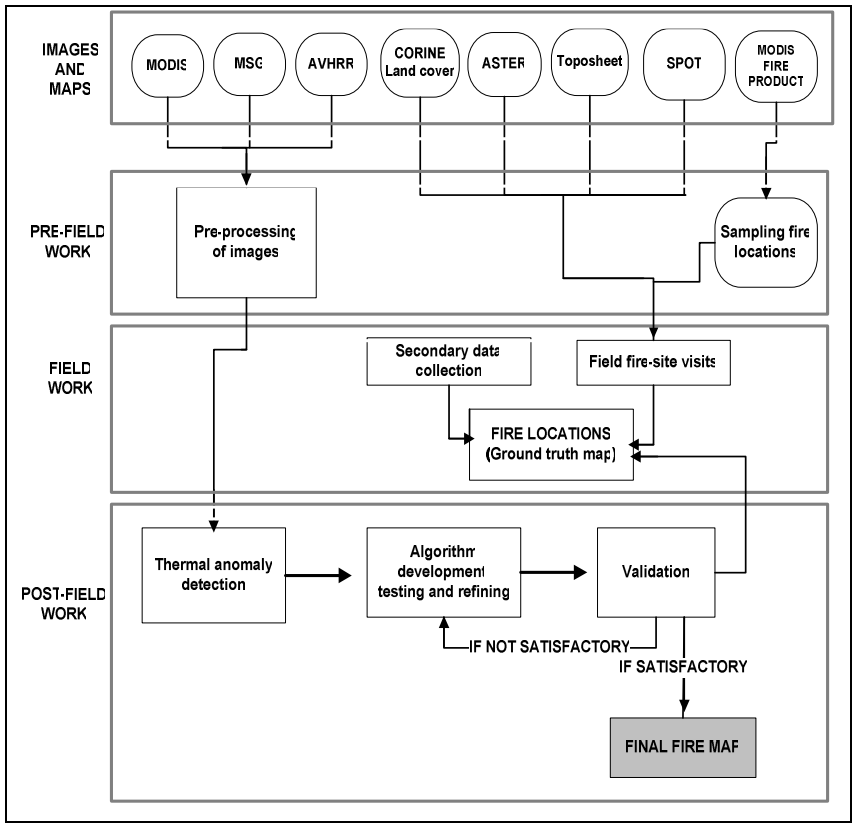

Figure 3.8 A schematic approach to research method

3.3 IMAGES AND MAPS USED

a) Images and maps used for field work

- Modis fire product*:* The 2006 fire locations were located with the help of the MODIS fire product available at MODIS Rapid Response System webpage at (http://rapidfire.sci.gsfc.nasa.gov/).
- Supporting field work data sets*:* Toposheets of Portugal (Military 1:50000) were used. The toposheets and ASTER images were reprojected to a common projection system. NDVI was extracted for the study area from SPOT images and classified broadly. The CORINE land cover map of 2003 and Michelin road map of Portugal were also used. These data were very vital for proper guidance and collecting accurate information in field.

b) Images and maps used for fire detection

This research has used MSG SEVIRI data; MODIS level 1b datasets and NOAA AVHRR level 1b datasets. The satellite images were acquired only for the dates of the field-visited fires. MSG provides 96 images per day for a particular place on the Earth. Therefore, this research has used 2592 MSG SEVIRI images. The MODIS and AVHRR data were searched for the same dates as MSG, however, due to their polar-orbiting nature, MODIS images a place 2 times each day and AVHRR once. Therefore, there were a number of fire occurrences for which there was no overpass. 11 MODIS images were acquired which were 24 incase of AVHRR. The acquisition of the images was as follows:

- MSG*:* The EUMETSAT at Darmstadt in Germany receives the MSG-1 SEVIRI data, which are processed and uplinked to HOTBIRD-6. ITC gets the data from HOTBIRD-6 with the help of a standard dish (A.S.M. Gieske, 2004). This study uses images from July 1st to September 15. The latitudinal and longitudinal extent of the images is 45^{o}N, 10^{o}W, 1^{o}W, and 35^{o}N. The images for each day at every 15 minute were acquired. The images have 153 rows and 115 columns. The pixel size is 3000.403m.
- NOAA AVHRR*:* The data has been downloaded from the website National Environmental Satellite, Data and Information Service (NESDIS)' at (http://www.class.noaa.gov/nsaa/products). The data type used was the Global Area Coverage (GAC) which is sub-sampled on board to 4km pixel separation at nadir specially for global fire monitoring. The data was acquired in the integer format.
- MODIS: This research uses the MOD021KM data product which contains calibrated radiances at 1km resolution. The data is acquired from the

Goddard Distributed Active Archive Centre (GDAAC) website at (http://ladsweb.nascom.nasa.gov/data/search.html). The dataset consists of geolocation information in the HDF file structure, which for every 1 km of MODIS observation defines the geodetic coordinates (WGS-84), the sensor zenith angle and azimuth, solar zenith angle and azimuth, and the terrain height. The calibrated radiances are represented as integers in 32-bit floating format for the thermal bands. For further details on the development of the product please refer to 'Level 1B Product Information and Status' (www.mcst.ssai.biz/mcstweb/L1B/product.html).

3.4 PRE-FIELD WORK

3.4.1 Sampling design and designing field work approach

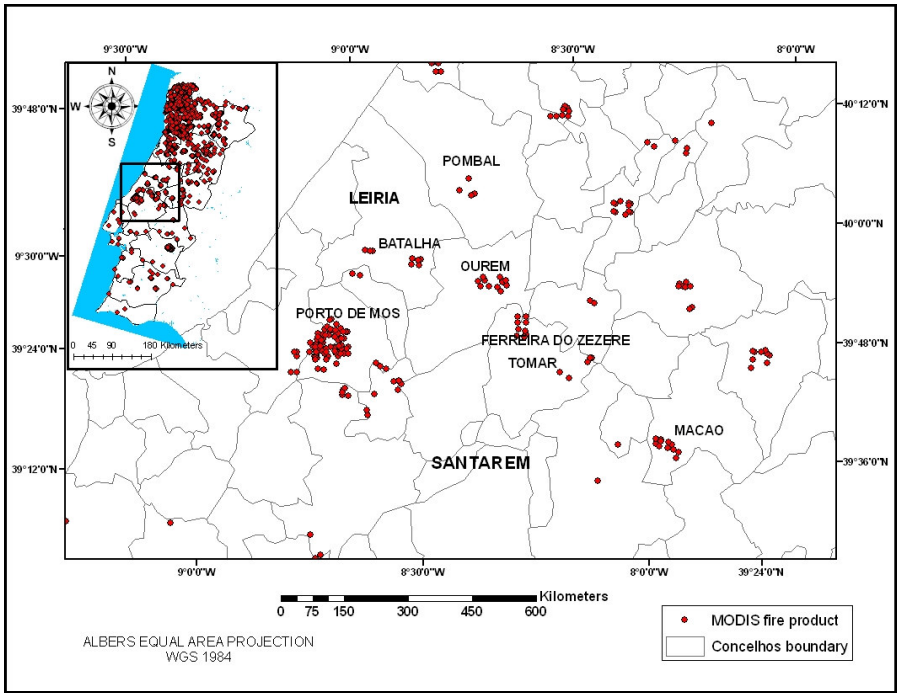

Figure 3.9 Sampling field work design

Figure 3.9 shows location of fires in Portugal (June- September, 2006) derived from the MODIS product of the rapid response system. The field work did not follow any particular sample design. On observing it is seen that the north-western region has more fires than the central region, however due to logistics and inaccessibility

because of the rugged terrain the north-western region was not selected. Ignoring the north-west fires the next region which has a large number of fires is central Portugal as demarcated in a box in figure 3.9. Therefore, the districts of Leiria and Santarem were chosen for field work. The field work visits closely followed the fires as seen in the MODIS product.

3.4.2 Pre-processing of images

The MSG, MODIS and NOAA AVHRR imageries went through a series of pre-processing steps before they were ready for the fire detection. Firstly the images had to be geometrically corrected. Secondly the data was calibrated so as to get the radiances from the digital number (DN). The radiances were further converted to brightness temperatures (degree Kelvin).

a) Geometric correction

- MSG: The pixel positions of the MSG image correspond to the angles of the geodetic coordinates due to the scanning characteristics. The geocoding of the image was done in the MSG data retriever at ITC. The values are used from the header file of the image.
- MODIS*:* The geometric corrections and removing of the Bow-Tie effect of MODIS images were done with the HEG tool which has been developed by the EOS and available to users since November 2004. The HDF EOS format which MODIS products use applies standards for attaching geolocation and temporal information to the data, this is not generally accessible to common softwares like Arc GIS, ENVI, ERDAS etc (http://edcdaac.usgs.gov/landdaac/tools). The HEG tool extracts information from the separate geolocation file, and geometrically corrects the image; it also helps in converting the format into a more common format. This study has used the geographic coordinate system (WGS 84) and converted the HDF EOS format to Geotiff in HEG.
- NOAA AVHRR*:* The data was georeferenced in ENVI 4.3 to the geographic coordinate system (WGS 84).

b) Conversion of DN to radiances and further to brightness temperatures

- MSG SEVIRI: The data is calibrated in the MSG Data Retriever developed at ITC.

  The radiance is calculated by

$$L_{wn} = slope * DN + offset$$

L_{wn} is the radiance in [$mWm^{-2}sr^{-1}(cm^{-1})^{-1}$]. DN is the digital number; the slope and offset are retrieved from the header files. The radiances from the thermal channels then converted to brightness temperatures calculated by the following equation.

$$T_b = \left[\frac{c_2 v_c}{\log\left(\frac{c_1 {v_c}^3}{R^{+1}} \right)} - B \right] / A$$

In the above equation T_b is the brightness temperatures (K); R is the observed radiances in [$mWm^{-2}sr^{-1}(cm^{-1})^{-1}$]; v_c is the central wave number of the channel. The radiation constants are given by [$c_1 = 2hc^2$ and $C_2 = hc/k_B$.]; c is the velocity of light, k_B is Boltzmann's constant and h is Planck's constant. The reflectance is calculated from the radiance values by the following formula

$$\rho_o = \frac{\pi L_{wn} {d_{SA}}^2 \Delta\lambda}{R_{TOA} \cos\theta}$$

Where ρ_o is the reflectance; R_{TOA} is the solar irradiance (Wm^{-2}) and cosθ is the cosine of the solar zenith and d_{SA} is the Earth-sun distance. L_{wn} is the radiance in [$mWm^{-2}sr^{-1}(cm^{-1})^{-1}$] (A.S.M. Gieske, 2004). For examples, details and steps of calculations please refer to appendix 1.

- MODIS*:* The calibrated radiances were obtained from the integer values by the following formula, header and offsets were obtained from the header.

$$\left[radiance\_scales(radiance\_Interger - radiance\_offsets) \right] * 1000000$$

The radiances ($W/m^2/m/sr$) are then converted to brightness temperatures by the *Planck's radiation Law*.

$$T = \left(\frac{hc}{k\lambda} \right) \frac{1}{\ln\left(2hc^2 \lambda^{-5} L^{-1} + 1 \right)}$$

L = radiance (Watts/m2/steradian/m)
h = Planck's constant (joule second)
c = speed of light in vacuum (m/s)
k = Boltzmann gas constant (joules/Kelvin)
l = band or detector center wavelength (m)
T = temperature (Kelvin)
For examples, details and steps of calculations please refer to appendix 2.

- NOAA AVHRR*:* The radiance was calculated from the Digital numbers (DN) by the following linear equation.

$$\text{Radiance (Ne)} = a_0 + a_1 * CE + a_2 * CE^2$$

In the above equation Ne is the radiance in $mW/(m^2 srcm^{-1})$, CE is digital number; a_0, a_1 and a_2 are thermal coefficients. The radiance was converted to brightness temperature using Planck's radiation equation: The temperature T_1 (Kelvin) is calculated with the following formula

$$T_1 = \frac{c_2 vc}{\ln\left(1 + \frac{c_1 v^3}{NE}\right)}$$

$$T_2 = \frac{T_1 - A}{B}$$

Where T_1 is temperature (K); c_1 and c_2 are the Plank radiation constants; vc is the centroid wave number; A and B are constants. For examples, details and steps of calculations please refer to appendix 3.

3.5 FIELD WORK AND DATA COLLECTION

Field work was done from September 28 till October 13 2006. The aim of the fieldwork was to acquire data on the occurrences of the fires of 2006 in Portugal, the date and time of the fire, the burnt area, their geographic locations and fire site characteristics. The burnt fire areas were visited on the basis of the sample designed prepared by the MODIS fire product.

- Secondary data collection

Secondary data were obtained from the municipal offices, the forest departments, the fire management local authorities and the fire men. The secondary data consisted of geographic locations of the fire, burnt area, time and date of the fire occurrence, and duration of the fire and some photographs of the fire. There were some municipalities which were very well advanced in burnt area mapping, which they did with GPS. However, there were some municipalities they recorded the burnt area location by drawing with the hand on a Toposheet. Therefore, it was very necessary to validate the data (location of fires) by field visits. Data was also collected on some meteorological parameters like the FWI index, drought index, and temperature and wind direction. The fire day temperature and fire day wind direction data was difficult to get and it was acquired for only 2 fires.

- Primary data collection and fire site visits

Field work was done with the help of pocket computer iPaq, GPS. The fires were mostly in higher altitudes and rugged terrain where forest was plenty with very small forest pathways. The Toposheets, ASTERS and road map which was in the iPaq helped in finding the right location to the fire sites. On reaching the sites the

secondary data geographic locations were validated with the GPS. The fire sites more than 20 hectares in size were visited in both the districts, since it was not possible to visit all the fires. The MODIS product was also validated. The false alarms in the MODIS product were noted and a few fire points which were not in the MODIS product were also digitised. It was not possible to validate the time of the fires; however, the duration of a few fires were validated by local interviews. General observations were also made on site characteristics including slope direction, vegetation, soil and distance of residences from the fire.

Utility of the field work: The data collected was vital for validation of the fire pixels detected by satellite data. The location of the fires, date and time of the fire occurrence, duration of the fire information are vital for observing and validating the thermal anomalies or hotspots in satellite data. The meteorological parameters were necessary to understand the cause of the fires. The wind direction data was necessary for validating shifts in fire pixels from their correct locations in the satellite images.

3.6 POST FIELD WORK

3.6.1 Thermal anomaly detection and selection of bands

On the basis of past researches and literature (chapter 2) fire detection is best with the help of the thermal bands located in the middle infrared and thermal parts of the spectrum. Therefore, this research uses these parts of the spectrum for fire detection. The fire detection procedures for the different satellite sensors are explained in the following sections.

a) MSG SEVIRI

The sensitivity of channels 1, 4, 5, 6, 7, 8, 9, 10, and 11 centred at 0.6 µm, 3.9 µm, 8.7 µm, 9.7 µm, 10.8 µm, 12.0 µm, and 13.4 µm to fires are checked. The first step in studying the image was to see whether there was a thermal anomaly for the fire location during the time of the fire. Based on literature about the performance of band 3.9 µm and personal observations of the thermal anomalies for the different fire pixels it is confirmed that band 3.9micron would be used for fire detection. The next task was to find other suitable bands for fire detection, this was done by taking advantage of the fact that different bands responded differently to hotspots. The following band test was performed to select appropriate bands for fire detection by calculating the difference in temperature between the 3.9 micron and, bands of longer wavelenghts the 8.7, 9.7, 10.8, 12.0 and 13.4 micron.

$$(ft_{3.9} - ft_{8.7 \text{ or } 9.7 \text{ or } 10.8 \text{ or } 12.0 \text{ or } 13.4}) - (nft_{3.9} - nft_{8.7 \text{ or } 9.7 \text{ or } 10.8 \text{ or } 12.0 \text{ or } 13.4})$$

Where t is the average brightness temperature (K), and the number in subscript is the band centre wavelength (λ), *f* stands for the fire pixels and *nf* for the non-fire pixels.

b) MODIS

The MODIS thermal channels used for detection of thermal anomalies are 20, 21, 22, 23, 24, 25 (MWIR) and 27, 28, 29, 30, 31, 32, 33, 34, 35, and 36 (TIR) located at wavelengths from 3.660 to 14.385 microns. Based on literature and personal observations the bands at 3.9-4 micron (21, 22, and 23) would be used for fire detection since their response to hotspots were higher than bands at longer wavelenghts. Band 36 at 13.6 micron had the least response to hotspots therefore the research would take advantage of the different responses of the bands 21, 22, 23 and 36 and use this as the base for fire detection. The following test was applied to calculating the difference in brightness temperatures for the bands at 3.9-4 micron and band at 13.6 micron:

$$(ft_{3.9} - ft_{13.6}) \text{ and } (nft_{3.9} - ft_{13.6}$$

Where, ft is the brightness temperature in Kelvin for the fire pixels; nft is the brightness temperature in Kelvin for the non-fire pixels, and the number in subscript is the band wavelength, which is channel 20, 21, 22 and 23 in case of MODIS.

c) NOAA AVHRR

NOAA AVHRR/3 has 3 thermal bands 3b (3.7 µm), 4 (11µm) and 5 (12 µm). The response of the different bands was observed for fire and non-fire pixels. The following test was applied to calculate the difference in brightness temperatures for band 3b (3.7 µm) and 4 (11 µm).

$$(ft_{3.7} - ft_{11}) \text{ and } (nft_{3.7} - ft_{11}$$

Where, ft is the brightness temperature in Kelvin for the fire pixels; nft is the brightness temperature in Kelvin for the non-fire pixels, and the number in subscript is the band wavelength.

Selecting bands for removing false alarms*:* The visible 0.6 µm band (MSG, MODIS and AVHRR) was selected to remove the false signals from clouds and highly reflective surfaces. During the daytime cloud pixels show fire like thermal properties. The TOA values in the visible channel are contributed by surface reflectance and atmosphere. The VIS 0.6 µm channel is good for cloud fraction estimation over the

land, because cloud free reflectance in this channel is not so high and therefore, the cloud affected pixels become prominent (http://www.eumetsat.in).

3.6.2 Algorithm development for detecting fire in satellite images

This research has detected fire pixels by differencing the abnormal temperature detections from the surrounding pixels which do not show thermal anomalies; by differencing the less sensitive and more sensitive bands; by differencing the thermal anomalies with the average temperatures of a pixel over the previous non-fire. The following sections explain the method applied for detecting MSG, MODIS and AVHRR fire pixels.

a) MSG SEVIRI

There were 2 methods developed for fire detection:

- Absolute thresholding
- Contextual thresholding

Absolute thresholding: The hotspot pixel diurnal temperature was compared to its normal diurnal TOA brightness temperatures. The normal diurnal TOA brightness temperatures were derived for the hotspot pixel by observing its temperature over the previous 10 days, which were non-cloudy. The average of the normal diurnal TOA brightness temperatures was calculated. The hot spot was then compared to the average diurnal TOA brightness temperatures. The following algorithm was applied for detecting the fire pixels:

$$pf = (df - dp) > 5K \text{ and } df > 35K \text{ and } VIS_{0.6} \leq 0.15$$

pf Is the possible fire pixel; df 3.9µm minus 13.4 µm (for the fire pixel); dp is the [Average (3.9 µm minus 13.4 µm)] for the fire pixel, but, during the previous 10 non-cloudy days) and VIS is the visible band at 0.6 µm. Diurnal temperature data for the area was not available therefore the average diurnal temperature 10 days prior to the fire was calculated.

In the first part of the algorithm the difference between 'band 3.9 and 13.4 of the hotspot pixel' and the 'average difference between band 3.9 and 13.4 of the hotspot pixel on previous 10 non-cloud days' must be more than 5K. The second condition states that the difference between band 3.9 and 13.4 of the hotspot pixel must be more than 35k. The third condition states that reflection of $VIS_{0.6}$ must be equal to or less than 0.15

Contextual thresholding: The fire pixel is extracted by comparing its temperature to its neighbour pixels or background temperature. The diurnal temperature of the non-fire pixels were observed for the study area and the following algorithm developed:

$$pf = t_{3.9} - t_{3.9nb\min} > 15K \text{ and } t_{3.9} > 315K \text{ and } t_{3.9} - t_{13.4} > 40K \text{ and } VIS_{0.6} \leq 0.15$$

pf is the possible fire pixel; t is temperature (K); $_{nbmin}$ is the minimum value of the neighbour pixel; The numbers in subscripts are bands used (3.9 µm and 13.4 µm) and VIS is the visible band.

In the first condition of the algorithm the difference between the temperature of a pixel and the minimum of its neighbour should be more than 15 to be qualified as a fire pixel. The second condition states the brightness temperature of 3.9 µm must be higher than 315K. The third condition states the difference in brightness temperatures between band 3.9 micron and 13.4 micron of the fire day should be more than 40K. The 4th condition is 0.6 µm must have a reflection of less than 0.15. A pixel must fulfil all the conditions in the algorithm in order to be flagged as a fire pixel.

b) MODIS

The brightness temperature of a fire pixel depends on 2 factors: The size of the fire and the temperature or intensity of a fire. A large fire (area wise) would have a higher brightness temperature than small fire (area wise). However, if the small fire has a high intensity it would have the same brightness temperature as the large fires and in this case both small and large fires would affect the same number of pixels with equal intensity. The fire area or intensity of fire is affected by weather factors as mentioned in section 3.2a. In other words a large fire test would be applied when the average temperatures of the area is high, since high temperature triggers fire. Therefore, on days having high temperatures the small fire tests cannot be applied since there would be a large number of false alarms. The small fire tests can only be applied on days when the average temperature is lower.

A small fire test would be applied under the following condition:

$$t_{21,22,23(\geq 80\% p)} \leq 310K$$

A large fire test would be applied under the following condition:

$$t_{21,22,23(\geq 50\% p)} \geq 310K$$

In the above conditions *t* is the brightness temperature (K), the numbers in subscript are the band numbers for MODIS, *p* stands for pixel. The conditions state that when there are 80% or more number of total pixels in the image having a temperature of

310K or less, (for bands 21, 22, 23 at 3.9 µm - 4 µm) then the small threshold test is applied. If 50% or more of the total pixels in the image have a brightness temperature of more than 310K then the large threshold test is applied. These conditions had the advantage that it was not necessary to know the local temperature conditions of the area, it was also not necessary to know the size of fire or intensity of fire. On the basis of the above conditions the type of thresholding test algorithm could be chosen. The disadvantage was however that cloud pixels could influence the large fires test.

- Large fires threshold test

$$pf = (T_{21} - T_{21nb\min} > 40K) \text{ or } (T_{22} - T_{22nb\min} > 40K) \text{ or } (T_{23} - T_{23nb\min} > 40K)$$

$$pf = (T_{21} > 350K) \text{ or } (T_{22} > 350K) \text{ or } (T_{23} > 350K)$$

$$p_f = (T_{21} - T_{36} > 100K) \text{ or } (T_{22} - T_{36} > 100K) \text{ or } (T_{23} - T_{36} > 100K)$$

$$p_f = R_1 \leq 0.2$$

Where, P_f is the Potential fire pixel; T is the brightness temperature; the number in subscript is the band number and R is reflectance. The night threshold test does not use the last condition stating reflection to be less than 0.2.

- Small fires threshold test

However, there are smaller fires which do not fulfill these conditions therefore the following thresholds are applied.

$$pf = (T_{21} - T_{21nb\min} > 15K) and (T_{22} - T_{22nb\min} > 15K) and (T_{23} - T_{22nb\min} > 15K)$$

$$p_f = (T_{21,} > 320K) and (T_{22} > 320K) and (T_{23} > 320K)$$

$$P_f = (T_{21} - T_{36} > 95K) and (T_{22} - T_{36} > 95K) and (T_{23} - T_{36} > 95K)$$

$$p_f = R_1 \leq 0.2 \; p_f = R_1 < 0.2$$

The night threshold test does not use the last condition stating reflection to be less than 0.2.

c) AVHRR

The following test was applied for detecting day fires. The pixel must fulfill all the conditions of the test to be claimed as a fire pixel during the day.

- Small fires test (day fires)

$$pf = (T_3 - T_{3nb\min} > 3K)$$

$$pf = (T_3 - T_4 > 10K) \text{ And } (T_3 > 315) \text{ And } (T_4 > 300)$$

$$pf = (R_1 \leq 0.1) \text{ and } (R_1 - R_2 \leq 0.1)$$

- Large fires test (day fires)

$$(T_3 > 325) \text{ And } (T_4 > 320)$$

$$pf = (R_1 \leq 0.1) \text{ and } (\mathrm{R}_1 - R_2 \leq 0.1)$$

- Small fires test (night fires)

$$pf = (T_3 - T_{3nb\min} > 3K)$$

$$pf = (T_3 - T_4 > 5K) \text{ And } (T_3 > 300) \text{ And } (T_4 > 290)$$

- Large fires test (night fires)

$$(T_3 > 320) \text{ And } (T_4 > 310)$$

In the above tests *pf* is the possible fire pixel; T is the brightness temperature (K); the number in subscript is the channel number of AVHRR. T_3 is temperature of channel 3b at 3.7 µm; T_4 is temperature of channel 4 at 11 µm.

The first condition states that the temperature of a pixel at 3.7 µm must be more than 3K than the minimum of its nearest neighbour. The second condition claims a difference in temperature between 3.7 µm and 11 µm to be more than 10K; and 3.7 µm to be more than 315 K; and 11 µm to be more than 300K. The 4th conditions remove the false alarms from clouds and other highly reflective surfaces.

The large fires test claims a temperature in channel 3b (3.7 µm) to be higher than 325 K and channel 4 (11 µm) more than 320K. In case of large fires test the difference between band 3.7 µm and band 11 µm is not considered since during very large fires there is not a large difference in thermal anomaly between the 3.7 µm and 10.8 µm.

Where *pf* is the possible fire pixel; T is the brightness temperature (K); the number in subscript is the band number. The 4th condition of the day fire test is not applied for the night fire test.

Please refer appendix 4 for the ILWIS scripts used, to apply the fire detection algorithms for MSG, MODIS and AVHRR images.

3.7 SUMMARY

This chapter gives an overview of the materials used for research and the methods adopted. The materials used were images and thematic maps. The study area was described and depicted, and a short overview was given on the forest fires in Portugal with some examples from the study area. The sample design and fieldwork approach was also discussed in this chapter. The tasks done during pre-processing of the images have also been elaborated namely the geometric correction and conversion of DN values to radiance and further to temperatures. The method used for selection of bands and fire detection have also been explained in this chapter.

4 RESULTS AND ANALYSIS

4.1 RESULTS OF FIELD WORK DATA COLLECTION

Figure 4.1 shows the burnt area (polygons) and burnt locations (point data). Most of the fires have occurred at altitudes more than 1000 meters. The fire location data for the high altitudes and rugged terrain are mostly in point locations.

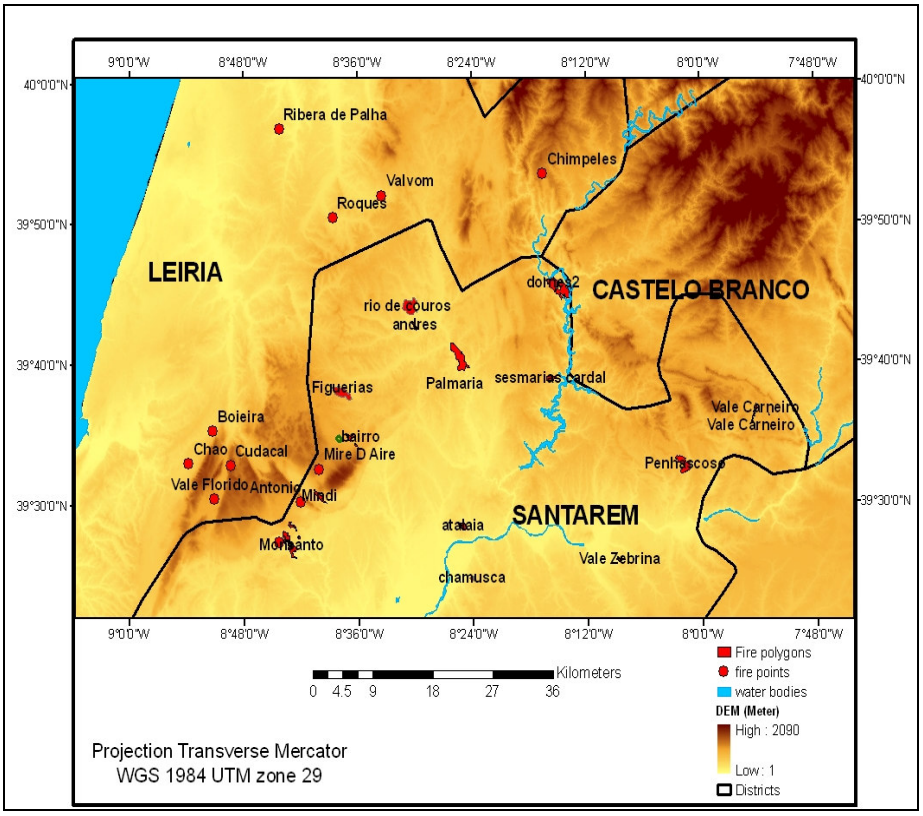

Figure 4.1 Fire locations collected during field work

Table 4.1 shows the results of the data collected during field work. The results obtained include a combination of secondary data collections, personal point location of fires and validation of the secondary data.

Table 4.1: Data collected from field work

Districts	Local	Fire locations Latitude	Longitude	Date (2006)	Time G.M.T	Duration Day/hr/min	Area (ha)
Leiria	BOIEIRA	39º 36' 33	W 008º 54' 01'	10-Aug	14:00	02d 10h 16m	NA
Leiria	CUDAÇAL	39º50' 38"	W 008º 06' 19'	5-Aug	11:45	00d 10h 16m	NA
Leiria	CHIMPELES	39º53' 32"	W 008º 16' 35"	11-Aug	16:53	01d 04h 16m	NA
Leiria	R.D PALHA	39º56' 48"	W 008º 44' 15"	6-Aug	15:25	01d 12h 15m	NA
Leiria	V. FLORIDO	39º30' 29"	W 008º 46' 44"	9-Aug	11:37	01d 01h 05m	NA
Leiria	M.D.P VALBOM	39º52' 02"	W 008º 33' 29"	16-Jul	16:26	00d 23h 04m	NA
Leiria	C. ANTONIO	39º32' 48"	W 008º 43' 06"	10-Aug	16:45	00d 02h 41m	NA
Leiria	C.ROQUES	39º50' 52"	W 008º 40' 14"	15-Jul	13:25	01d 08h 35m	NA
Leiria	C.CHÃO	39º32' 38"	W 008º 50' 19"	8-Aug	13:13	00d 11h 29m	NA
Leiria	B. MIRA D´AIRE	39º32' 48"	W 008º 43' 06"	6-Aug	13:44	02d 11h 51m	NA
Leiria	C. POMBAS	39º30' 29"	W 008º 46' 44"	9-Aug	11:30	00d 13h 44m	NA
Santarem	FIGUEIRAIS	39º 38' 6"	W 8º 37' 54"	17-Jul	11:50	00d 07h	261
Santarem	R. COUROS	39º 44' 7"	W 8º 30' 40"	7-Aug	11:45	00d 08h	306
Santarem	PEDERNEIRA	39º 34'19"	W 8º 36' 16"	10-Aug	15:19	00d 05h	14
Santarem	BAIRRO	39º 34'54"	8º 36' 57"	14-Aug	14:24	00d 4h	50
Santarem	PALMARIA	39º 40'38"	W 8º 25' 30"	4-Sep	13:33	00d 15h	374
Santarem	ANDREAS	39º 43' 2"	W8º 30' 25"	4-Sep	15:55	00d 05h	23
Santarem	V. ZEBRINHO	39º 26' 2"	W 8º 8' 45"	14-Jul	18:38	00h 03h	24
Santarem	DORNES	39º 45'20"	W 8º 14' 29"	26-Jul	13:39	00h 12h	438
Santarem	MURETA	39º 30'37"	W 8º 40' 04"	6-Aug	9:15	00d 6h 30m	74
Santarem	CARDAL	39º 39' 2"	W 8º 15' 52"	6-Aug	12:40	00d 03h	70
Santarem	MONSANTO	39º 27'43"	W 8º 43' 30"	6-Aug	13:04	00d 12 h	223
Santarem	CORTICAL	39º 28'41	W 8º 5'30"	6-Aug	13:30	00 10 h	288
Santarem	CARREGUEIRIA	39º 24'45"	W 8º 24' 9"	11-Aug	13:41	00d 03h	23
Santarem	ATALAIA	39º 28'25"	W 8º 27' 28"	22-Aug	15:42	00d 03h	58
Santarem	PENHACOSA	39º 32'48"	W 8º 1' 50"	4-Aug	10:37	00d 06h 30m	244
Santarem	V. CARNEIRO	39º 36'41"	W 7º 54' 28"	6-Sep	15:55	00d 05h	37

(NA: Not available)

Limitations in field data collected: No data on burnt area was obtained in Leiria since the burnt area mapping usually begins after October 2006. The burnt area knowledge is necessary for analyzing the thermal anomaly and performance of fire detection algorithm. It would have been good if information on 2006 fires were obtained for the entire country; however such data is not yet available. The time of fire start in

some fire cases were not very accurately documented, this inaccuracy is observed in the start time of thermal anomaly by the MSG sensor.

4.2 THERMAL ANOMALY DETECTION AND SELECTION OF BANDS

4.2.1 MSG

To detect the bands response to hotspots the diurnal brightness temperature profile (K) for the entire day (96 images) for the hotspots were observed.

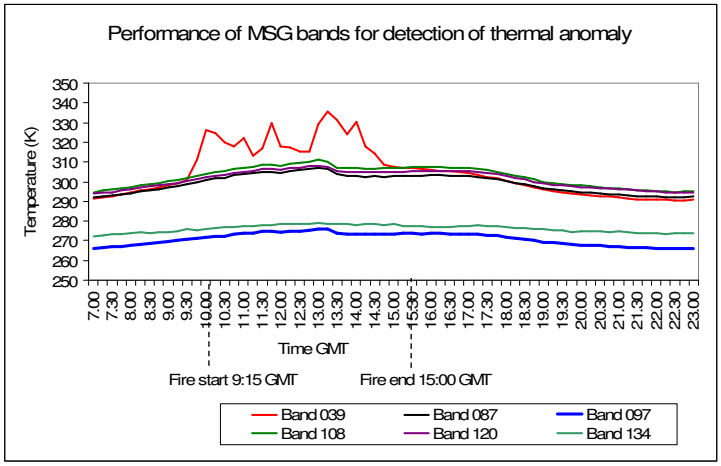

Figure 4.2 Thermal anomaly of 1 fire pixel (MSG infrared bands) Example: Penhacosa fire 04-August, 2006.

Figure 4.2 shows the performance of the different bands for detecting thermal anomaly for 1 fire pixel. The graph shows the brightness temperature in Kelvin for the fire which occurred in Penhacosa. The fire had started at 9:15 GMT and lasted untill 15:00 GMT; this is clearly evident in the figure. As observed in the figure the performance of 3.9 µm is the best. The 10.8 µm, 12.0 µm and 8.7 µm band performance is nearly the same. The 9.7 µm and 13.4 µm are the 2 bands which have a low sensitivity to fires. Therefore, it is evident that bands located at the windows part of the spectrum namely at 3.9 µm, 8.7 µm, 10.8 µm and 12.0 µm were more sensitive to forest fires. Please refer to appendix 5 for thermal anomaly detection (MSG 3.9 µm).

a) Analysis of 3.9 micron performance

Figure 4.3 shows response of 3.9 micron band during the day and night for the same fire pixel (field site visited fire pixel). During the day (image 11:00 GMT), due to receiving sun's reflected energy and Earth's radiant energy the image is more brighter but at night (23:45 GMT) the overall image is more darker. Though the absolute temperature of the hotspot is hotter during the day due to receiving energy from the Sun and Earth but there are larger false alarms from background pixels due to solar heating. During the night the hotspot clearly stands out as compared to the background pixels therefore, the fire detection for a pixel is better during the night than during the day.

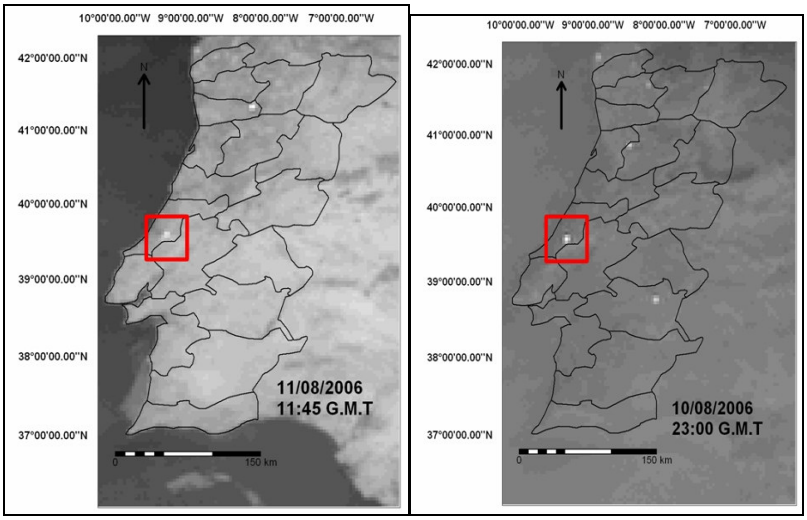

Figure 4.3 Response of 3.9 µm to day fire and night fire

b) Calculating difference in temperatures between 3.9 µm and other bands

On the basis of results in figure 4.2 and supported by literature in chapter 2 it can be said with no doubt that 3.9 µm is the best band for fire detection. The difference in temperatures (K) between band 3.9 µm and bands of the longer wavelenghts at 8.7 µm, 9.7 µm, 10.8 µm, 12.0 µm and 13.4 µm was calculated. The aim was to see the deviation between the 'average temperature difference between 3.9 µm and the longer wavelenghts' for fire and non fire pixels and for day and night fires. Table 4.2 shows the results of an average of 20 fires. It is seen that the maximum difference is for 9.7 µm followed by 13.4 µm. The same trend is observed for the non-fire pixels. However, on differencing the non-fire pixels with the fire pixels it is seen that the

maximum difference is for 13.4 µm, in other words it is the least sensitive band. 10.8 µm was most sensitive followed by band 12.0 µm and band 8.7 µm. The day and night fires showed the same results. On the basis of the above discussions it is seen that band 3.9 µm is most sensitive to forest fires followed by 10.8 µm, therefore, 10.8 µm is selected for comparison with band 3.9 µm.

Table 4.2: Temperature difference (K) between 3.9 µm and other bands

CATEGORIES	$ft_{3.9} - ft_{8.7}$	$ft_{3.9} - ft_{9.7}$	$ft_{3.9} - ft_{10.8}$	$ft_{3.9} - ft_{12.0}$	$ft_{3.9} - ft_{13.4}$
Average difference (K) (day fire pixels) (A)	14.08	43.86	10.27	11.90	36.02
Average difference (K) (day non-fire pixels) (B)	1.79	31.85	1.87	0.43	23.34
Difference (A-B) (K)	12.29	12.01	12.14	12.32	12.68
Average difference (K) (night fire pixels) (C)	9.82	35.54	5.71	7.91	29.66
Average difference (K) (night non-fire pixels) (D)	-0.95	25.89	3.80	3.42	15.18
Difference (C-D) (K)	10.76	9.65	9.50	11.32	14.47

c) Comparison of band 3.9 µm and band 10.8 µm

In order to compare the sensitivity of the 2 bands to fires a night fire image was selected. This is because during the day 3.9 µm is influenced by solar radiation, but at night it is only influenced by the Earth radiation just the same as 10.8 µm.

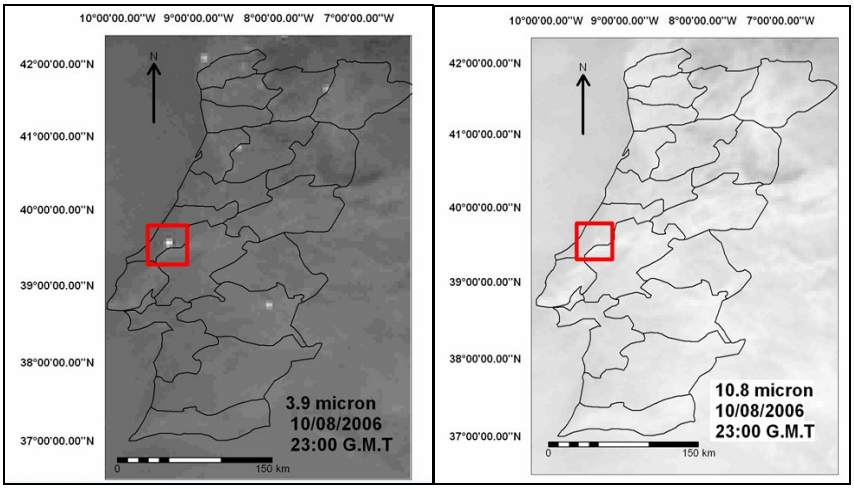

Figure 4.4 Response of 3.9 µm and 10.8 µm to night fires

Figure 4.4 shows the response of 3.9 µm and 10.8 µm to night fires. The red circled bright pixel shows a fire which occurred in Boieira, it was a fairly large fire having a burnt area of approximately 400 ha (estimated). It is clearly seen that 3.9 µm is more sensitive than 10.8 µm, the temperature of the bright pixel in the red box in the 3.9 µm image is 335 K, whereas the same pixel has a temperature of 310 K incase of the 10.8 µm image. An added explanation to the better performance of 3.9 micron MSG band is that it is very sensitive to sub-pixel hot spot areas and this makes it very useful for detection of active fires. Band 10.8 micron is not sensitive as 3.9 µm for detection of sub-pixel fires; however during very large fires it shows nearly the same brightness temperatures as band 3.9 µm. Therefore band 10.8 shall not be used for fire detection since small fires would not be detected due to poor response to sub-pixel hot spots, and if a low threshold is applied it would lead to generation of false alarms. On the basis of the above results it was decided to detect fires by using the most sensitive and least sensitive bands namely the 3.9 µm and 13.4 µm. It was next necessary to know the difference in sensitivity of 3.9 µm and 13.4 µm to forest fires because this would be necessary for developing the algorithm.

d) The difference in sensitivity between 3.9 µm and 13.4 µm to forest fires:

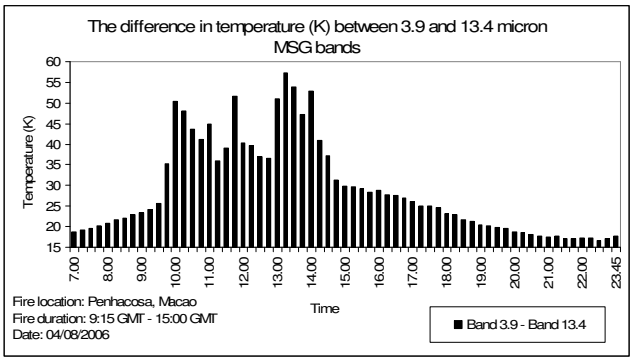

Figure 4.5 Difference in sensitivity between 3.9 µm and 13.4 µm

The 27 fires were checked for observing this difference. Figure 4.5 is an example of 1 fire which shows that the difference between 3.9 µm and 13.4 µm during non-fire conditions is 10K -25K, but during fire the difference 40K – 60 K.

4.4.2 MODIS

To detect the bands response to hotspots the brightness temperature (K) for the fire pixels were observed for all the infrared bands. Figure 4.6 shows the thermal anomaly for MODIS day (Terra 10:40 GMT) and MODIS night (Aqua 10:40 GMT). The black bars show the temperature (K) for fire pixels and the white bars show the temperature (K) for non-fire pixels. The bands at 3.9-4 µm are more sensitive to fires than other bands. Please refer to appendix 6 for thermal anomaly detection of the different fires for MODIS.

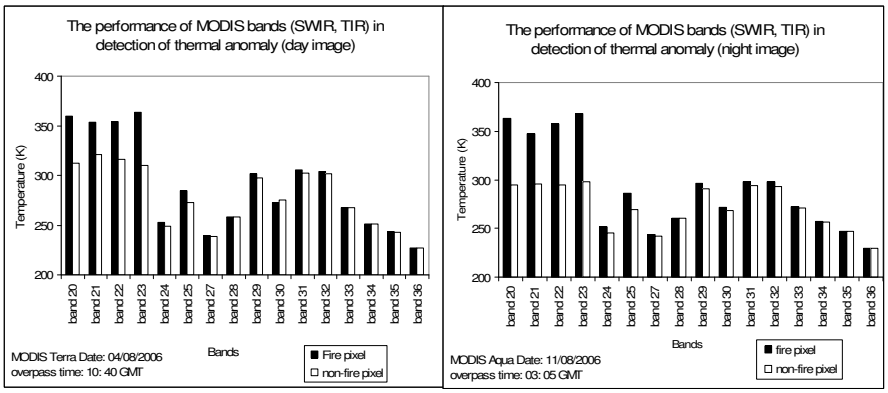

Figure 4.6 Thermal anomaly of MODIS bands (Day and night fire)

This results of some bands being sensitive than others is explained on the basis of their position in the spectrum, whether at shorter or longer wavelenghts and their positions in terms of the atmospheric absorption bands or atmospheric windows as explained in section 2.1. Figure 4.7 shows the mean brightness temperatures of all the pixels for 1 image for the various bands of MODIS, the bands at the absorption parts of the spectrum have lower brightness temperatures than bands at atmospheric windows.

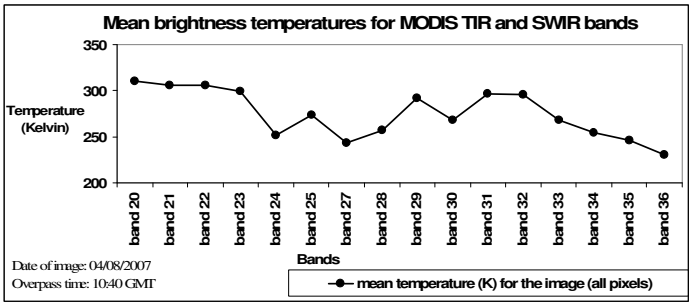

Figure 4.7 Mean temperatures (K) for the MODIS SWIR and TIR bands

a) Calculating difference in temperatures between most sensitive and least sensitive band

The same principal for fire detection is applied to MODIS as incase of MSG. The bands having highest sensitivity were selected (band 20, 21, 22, 23 at 3.6-4 micron) and band having the least sensitivity was selected (band 36 at 13.6 µm).

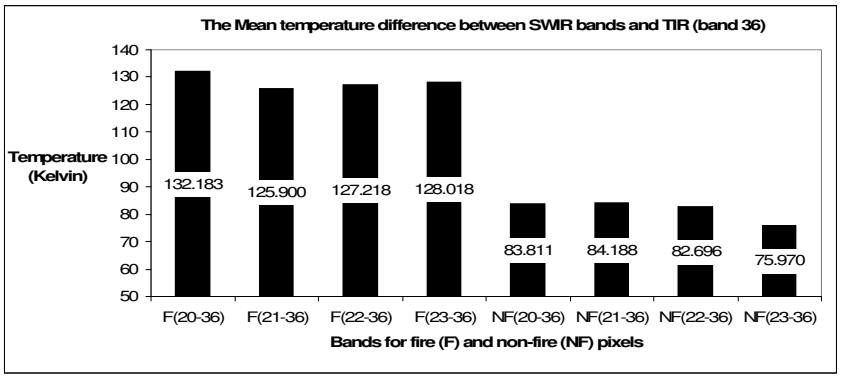

Figure 4.8 Difference in thermal response between 3.9 µm and 13.6 µm

Figure 4.8 shows the average difference in temperature (K) for fire and non-fire pixels between 3.9 µm and 13.6 µm. MODIS images of 4 different dates were tested and the average temperature difference is shown in figure 4.9. The bands at approximately 3.9 µm include MODIS bands 20, 21, 22 and 23 and the temperature of each band was differenced with band 13.6 µm. The results show that for a fire pixel the temperature difference is more than 100 (K) and for non-fire pixels it is below 90K. However, for smaller fires the difference in fire pixels is more than 80 (K) and difference in non-fire pixels is less than 50 (K).

4.2.3 AVHRR

There are not many options with regards to choice of bands incase of AVHRR. AVHRR/3 has 3 infrared bands 3b, 4 and 5 at 3.7 µm, 11 µm and 12 µm respectively. Figure 4.9 shows the thermal anomaly for day and night fires. The 3.7 µm has a higher response to fire than 11 µm and 12 µm. Figure 4.10 depicts the difference in brightness temperature between 3.7 µm and 10.8 µm for fire and non-fire pixels. The difference in temperature between these 2 bands is least for very large fires. There is however a larger difference in temperature between the 2 bands in case of small fires since band 3.7 µm shows a high anomaly even when a small fraction of the pixel is covered by fire. The temperature of 3.7 µm is highly affected by the solar zenith angle and scan angle as mentioned in chapter 2 and therefore it is

very difficult in developing a threshold. Please refer to appendix 7 for thermal anomaly detection for the different fires with AVHRR.

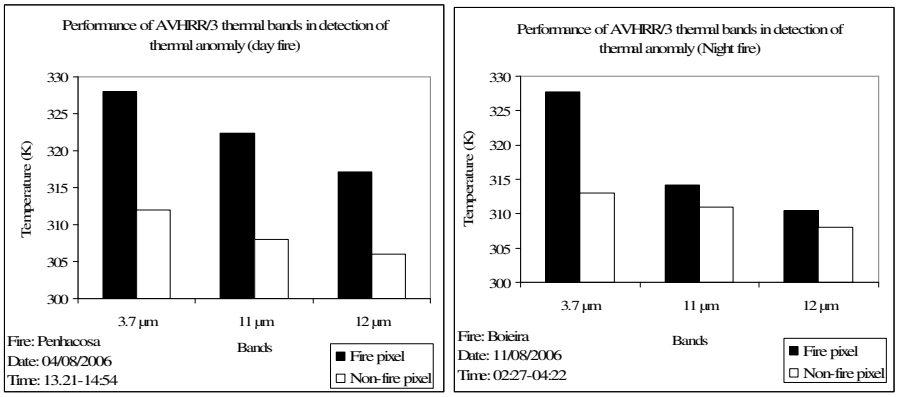

Figure 4.9 Thermal anomaly detection for AVHRR (day and night fire)

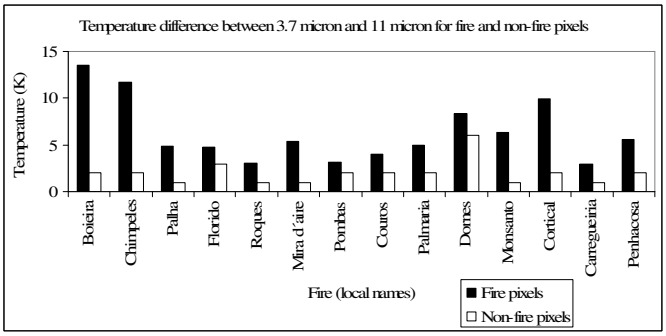

Figure 4.10 The difference in temperature (K) between 3.7 µm and 11 µm

Figure 4.10 shows the difference in temperature (K) between 3.7µm and 11µm. The difference between the 2 bands is lower for very large fires. Generally the temperature difference between the 2 bands ranges between 5-10 K. There are a large number of non-fire pixels too which have a difference in this range leading to a large number of false alarms. However, this trend is not consistent since 3.7 µm is very sensitive to solar zenith angle and scan angle of the sensor.

4.3 RESULTS AND VALIDATION

4.3.1 Performance of the algorithms

a) MSG

Contextual algorithm: The algorithm has 4 conditions. Considering the 1st condition, which states that difference between the temperature of a pixel and the minimum of its neighbour should be more than 15 to be qualified as a fire pixel this led to large number of false alarms along the boundaries of cold and hot surfaces, for example the coast line pixels were extracted as fire pixels. In the next step when 2 more conditions were added, which claimed (a) temperature of the fire pixel should be more than 315 K (b) difference between 3.9 µm and 13.4 µm fire pixel should be more than 40K. The number of false alarms which were there for the 1st condition was removed. There were a few suspected false alarms. The study does not have field data for the entire country Portugal however following the assumption that a pixel is a false alarm if it is flagged as a fire pixel for less than 3 consecutive MSG overpasses. Figure 4.11 is an example of a false alarm.

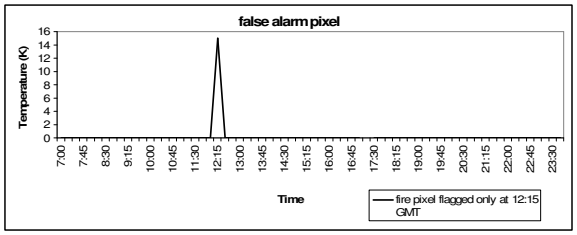

Figure 4.11 showing suspected false alarms

After adding the 4th condition along with the above 3 conditions the algorithm worked very well. The added condition was that a pixel should have a reflection of less than 0.1 in the VIS0.6 band. This removed the false alarms from clouds and highly reflective surfaces.

It was necessary to check if the fire pixel was flagged as a fire pixel throughout the duration of fire. The duration of the fire event was acquired from field data. The algorithm worked very well. Figure 4.12 shows the number of times fire pixels are flagged as fire, this is an example of the Penhacosa fire which started at 9:30 G.M.T and ended at 15:00 G.M.T. This was tested for all the fires and the results were satisfactory. Please refer to appendix 6 for graphs showing the frequency of fire pixels being flagged for the different field visited fires.

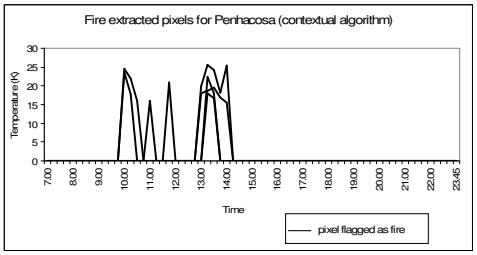

Figure 4.12 Number of times a pixel is flagged a fire

Absolute algorithm: There were 3 conditions for a pixel to be flagged as a fire. (a) The difference between band 3.9 and 13.4 of the hotspot pixel must be more than 35k; (b) The difference between 'band 3.9 and 13.4 of the hotspot pixel' and the 'average difference between band 3.9 and 13.4 of the hotspot pixel on previous 10 non-cloud days' must be more than 5K; (c) that reflection of 0.6 µm must be equal to or less than 0.15. The first condition led to a large number of false alarms. This is because during a hot day around noon the difference between band 3.9 and 13.4 was more than 40 K for a large number of pixels. However, after applying the 2nd and 3rd conditions this algorithm worked very well.

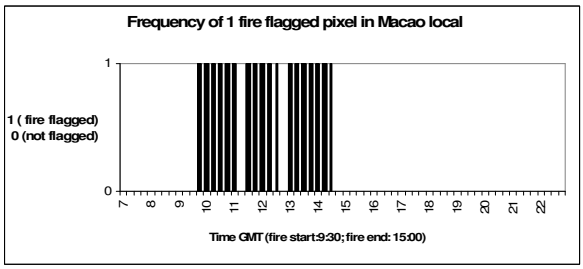

Figure 4.13 Number of times a pixel is flagged a fire

Figure 4.12 and 4.13 are the results of the same fire after being tested with contextual and absolute thresholding algorithm respectively. Both the contextual and absolute algorithms worked equally well and figure 4.14 shows the fire pixels flagged with both the algorithms. The map shows fires only for the dates of the field visited fire sites. In order words the map shows fires of Portugal which occurred on July (14, 15, 17 and 26) August (4-11, 14 and 27) and September (4 and 6).

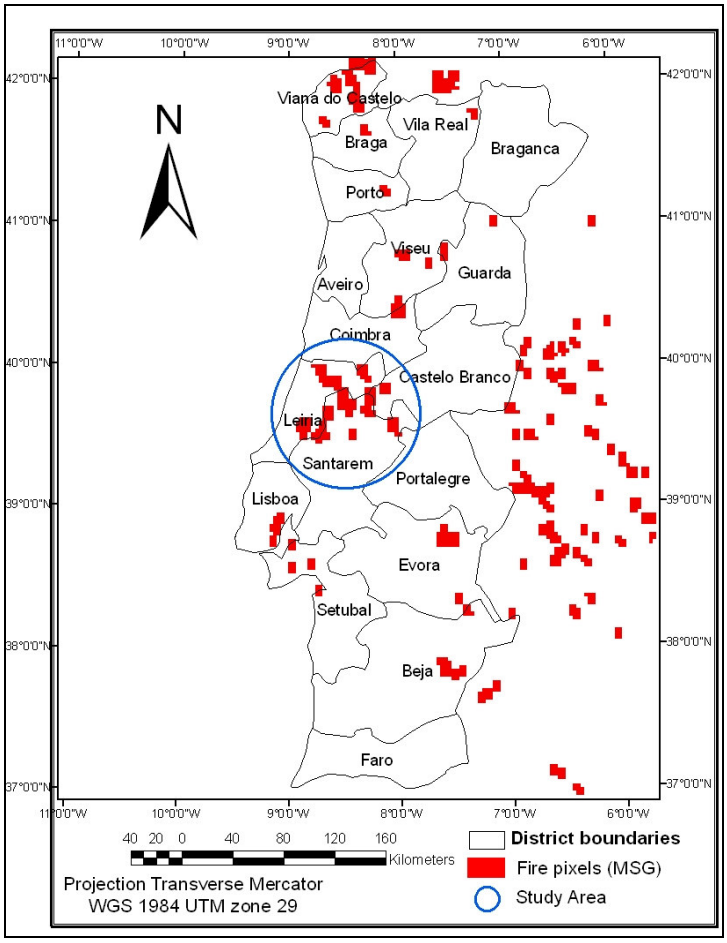

Figure 4.14 Map showing MSG fire pixels for selected days

b) MODIS

The algorithms used band 21, 22 and 23 (3.9 µm- 4 µm) for detecting forest fires. Band 20 (3.6 µm) was extremely noisy; and generated a large number of false alarms. This band is good for detecting very large fires or fires generating a high signal, however it did not perform well for small fires since when a low threshold was applied there were many hotter areas which showed false alarms.

Performance of the large fires algorithm: The large fire test had 3 conditions to be fulfilled. The first condition stated that the fire pixel for 3.9 µm must be more than 350K; the second claimed a difference in temperature of fire pixel between bands 3.9 µm and 13.6 µm to be more than 100 K; the third condition was that reflection at 0.6

µm must be lower than 0.2. After applying all the conditions the algorithm worked very well and generated no false alarms.

Performance of the small fires algorithm: The small fires test had the same conditions of the large fire test except that it had lower threshold values. The small fires test did generate a few false alarms incase of band 21 and band 22 (3.9 µm), however, band 23 (4 µm) performed better.

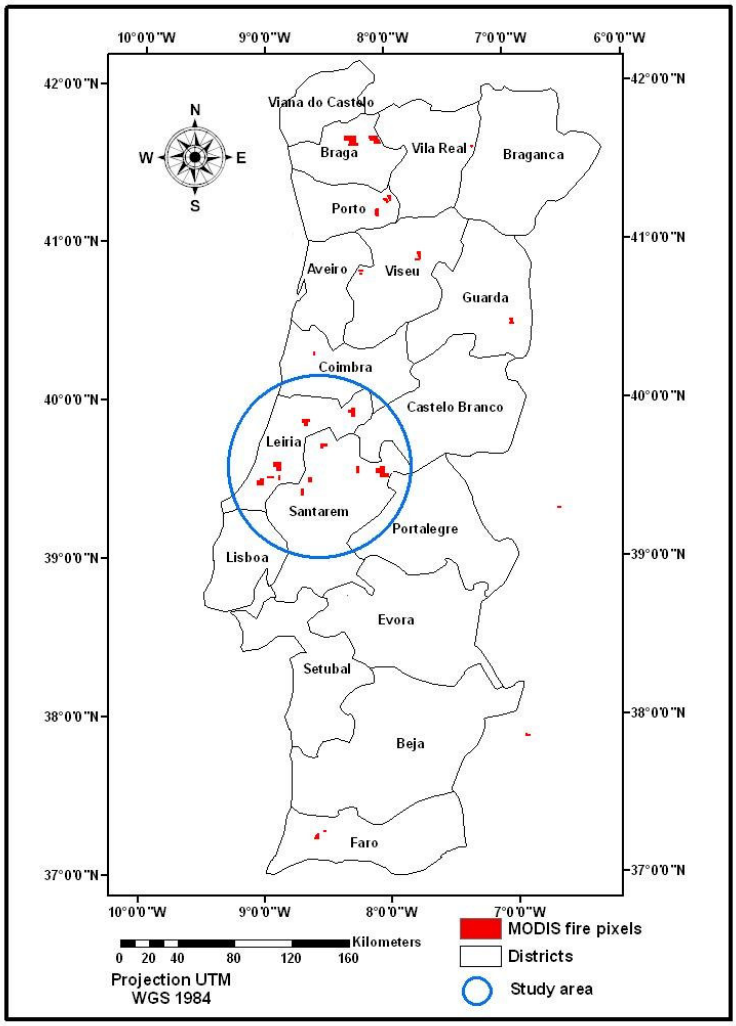

Figure 4.15 Map showing MODIS fire pixels for selected days

c) Fire detection with AVHRR

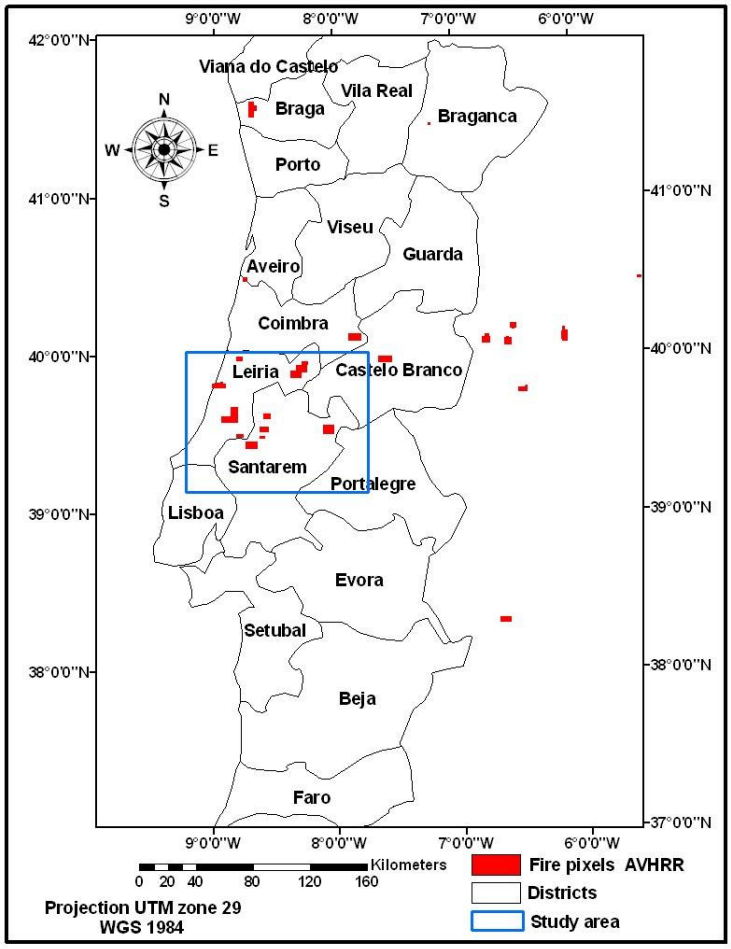

Figure 4.16 Map showing MODIS fire pixels for selected days

The AVHRR night fires test performed better than the day fire test, since 3.9 µm had a higher response to fires than 10.8 µm, further there is not much problem of false alarms during the night. The day fire test had the problem of false alarms and this problem arose mainly when flagging small fires, however incase of large fires there was no such problem.

4.3.2 Validation of the fires detected

The fires detected incase of MSG, MODIS and AVHRR were validated with the field visited fires. Since data for the entire country was not available therefore the first idea was to use the MODIS product to validate the fires detected in this research. However, it was first necessary to validate the MODIS product.

a) MODIS product

The MODIS product was validated with the field work data. Figure 4.17 shows the results of the validation. The results are not very satisfactory.

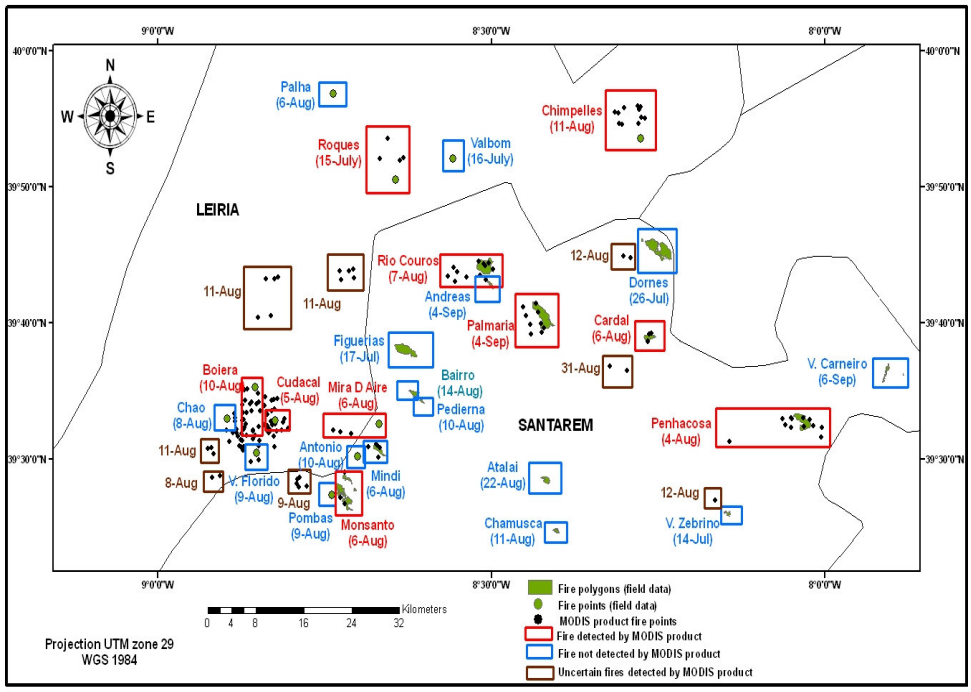

Figure 4.17 Validating the MODIS product with visited fire sites

- The points and polygons (field data) in blue boxes show the fires which the MODIS product did not detect. On checking the location (coordinates), acquisition date and time, and confidence levels of the MODIS fire points it was seen that 17 fires out of the 27 field visited sites were not detected by MODIS.
- The red boxes encircling the MODIS product points along with the green fire points and polygons (field data) show the fires which the MODIS product has detected. From 27 fires only 10 fires were detected.

- The brown box encircling the MODIS product fire points are the points for which no field data is available. There maybe 2 explanations for this:
  (a) The points are false alarms. (b) The field work data has failed to collect these fire points. The latter is unlikely since care was taken to collect data on all fires larger than 20 (ha), the fire points in question cannot be fires smaller than 10 (ha), since the performance of the MODIS product in fire detection shows the all the 10 fires detected in figure 33 are larger than 300 (ha).

Therefore, the MODIS product shall not be used for validating the fires detected in this research. However, it shall be compared with the fires detected in this research since the MODIS product is an accepted commercial fire product and it would be useful to see how the algorithms developed in this research perform with relation to the MODIS product. This would also be useful to compare the 3 sensors for fire detection. However, the MODIS points encircled in brown shall be removed for further analysis since they are uncertain fires.

b) Validation of MSG fires detected

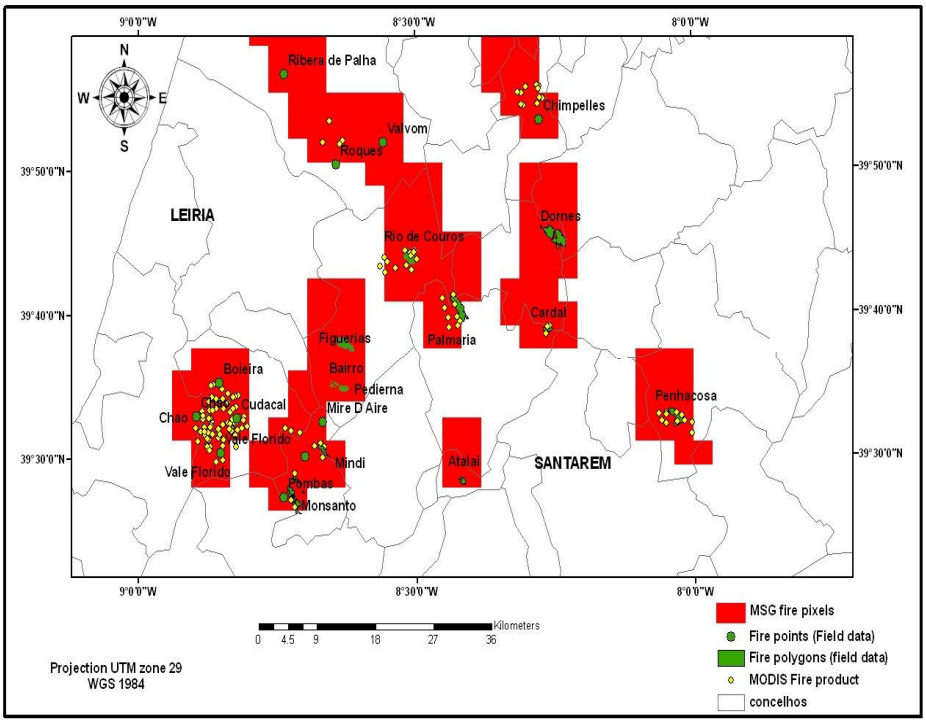

Figure 4.18 Comparing MSG fire pixels with field data and the MODIS product

The possible fire pixels which were flagged by the satellite images were validated with the ground truths obtained from field work. The fires in the field study area (Leiria and Santarem) were validated. Figure 4.18 shows the MSG fire pixels overlaid with the field data and the MODIS product fire points. Out of the 27 field visited fires, 2 fires were caused by thunder and lighting and had cloud cover due to which it was not possible to detect the thermal anomaly. The algorithm was therefore tested with 25 fires. The satellite data has flagged 22 fires out of the 25 field visited fire sites. The 3 fires which were not flagged were smaller than 25 (ha) and short duration of fire (2-3 hours) which caused low temperatures not high enough to fulfil the conditions of the thresholding algorithm.

c) Validation of MODIS fires detected

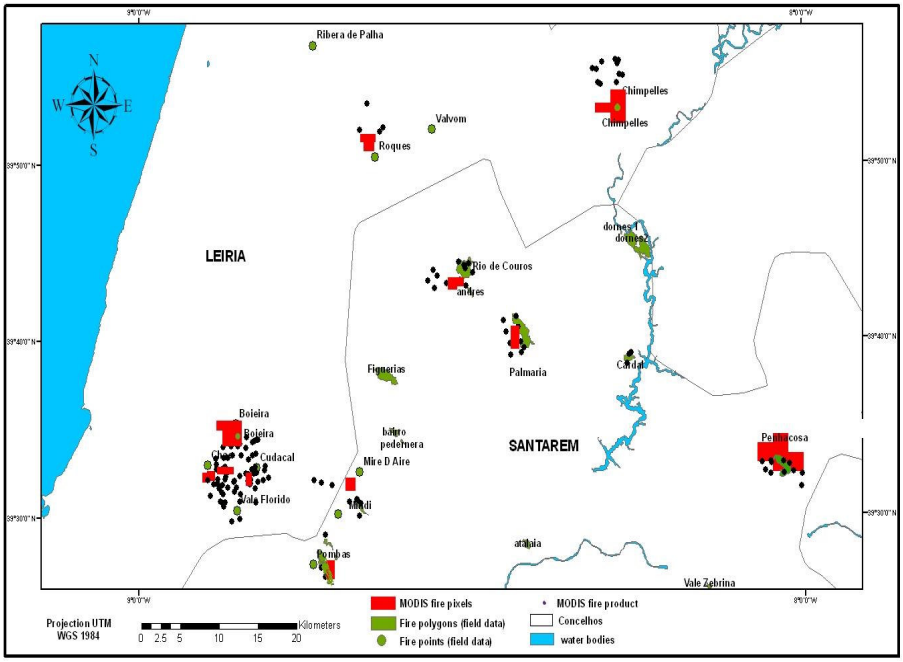

Figure 4.19 Comparing MODIS fire pixels with field data and the MODIS product

There were only 14 fires out of the 27 which had an overpass image. Therefore the algorithm was tested for the fire dates of these 14 fires. Out of the 14 fires 9 fires were detected with the algorithm and 5 fires were not detected. The fires that were detected in Santarem had burnt areas of more than 250 (ha). The burnt area data of Leiria was not available but the fires that were detected had fire durations of more than 1 day, therefore inevitably leading to high brightness temperatures. Comparing

the performance of the algorithm with the MODIS product it is seen that it detected 1 fire less than the MODIS product.

d) Validation of NOAA AVHRR fires detected

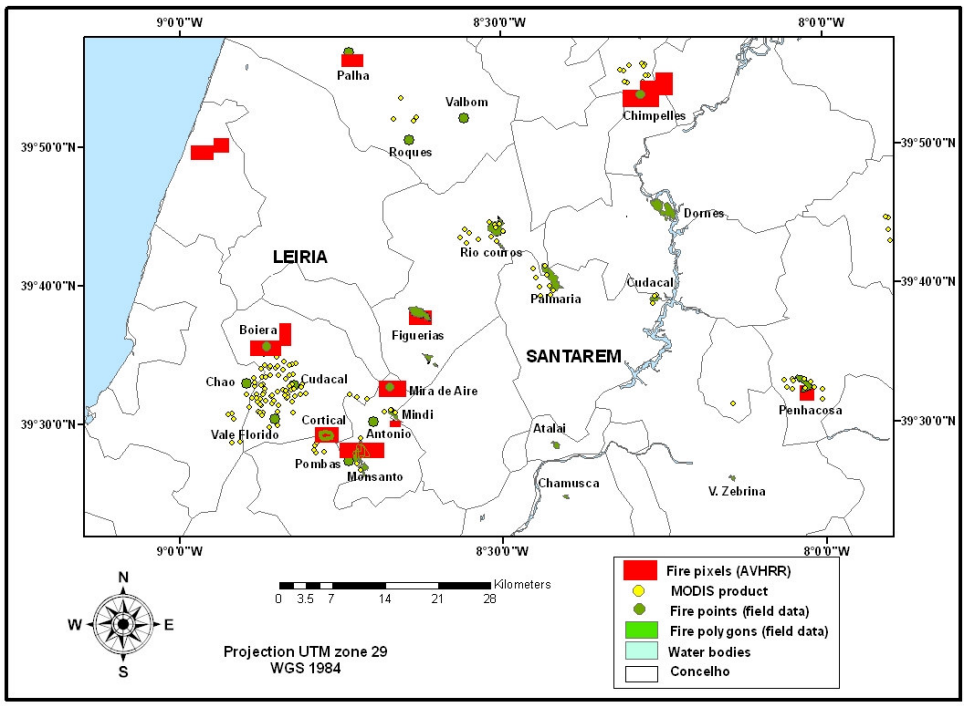

Figure 4.20 Comparing AVHRR fire pixels with field data and the MODIS product

24 images were tested and figure 4.20 shows the results. 9 fires have been flagged as fires, out of which 7 where flagged by the night threshold algorithm and the day threshold test flagged only 2 very large fires. There are 2 detected fire pixels near the coast but there is no field data to validate it, and it might also be that they are false alarms. Comparing the fire with the MODIS product it is seen that the MODIS product has not flagged the fire in central Santarem, Ourem.

4.4 COMPARISON OF THE 3 SENSORS FOR FIRE DETECTION

4.4.1 Comparing the response of the sensors to thermal anomaly

The fire detection capability and performance of a sensor depends on their response to fires and hotspots. This section would compare the different bands of the 3 sensors and their temperatures during a fire. The temperature of MSG would be compared with AVHRR and MODIS at the same time (or nearly same time) as of the AVHRR and MODIS satellites overpass and for the same fire pixel. If there is a time difference between MSG and, AVHRR and MODIS it is not more than 10 minutes since there is a MSG image for every 15 minutes.

a) comparing MSG and AVHRR

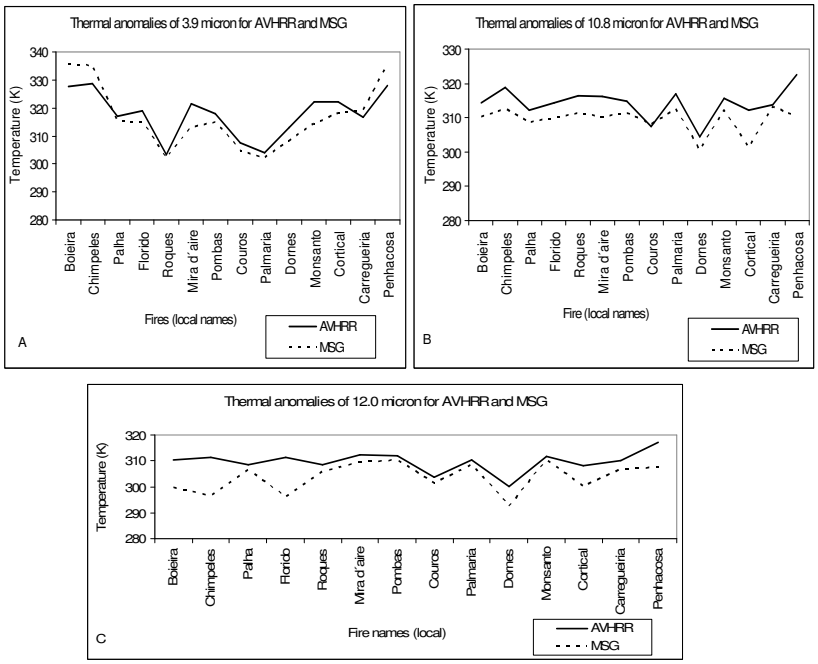

Figure 4.21 Comparing thermal anomalies for MSG and AVHRR, (A) 3.9 micron (B) 10.8 micron (C) 12.0 micron

It is necessary to know the saturation temperatures for the different bands in the 3 sensors. The saturation temperature for AVHRR 3.9 micron is 320-331 (K) (GIGLIO.; et al., 1999). MSG bands 3.9 µm, 10.8 µm and 12.0 µm saturates at 335K (CIHLAR et al., 1999). MODIS Channel 22 (3.9 µm) saturates at 335 and channel

21 (3.9 µm) saturates at 500K (Lim; et al., 2001). Figure 37 (A) shows the thermal anomaly comparison between MSG and AVHRR for 3.9 µm for 14 fires. The temperature of MSG is generally lower than AVHRR for fires which have a brightness temperature below 325 (K). Incase of larger fires with brightness temperature above 325 (K) the MSG shows a higher temperature since AVHRR has a low saturation temperature. In figure 37 (B) and (C) the 10.8 µm and 12.0 µm of AVHRR is higher than that of MSG since fires rarely reach the saturation temperature incase of these bands.

b) Comparing MSG and MODIS

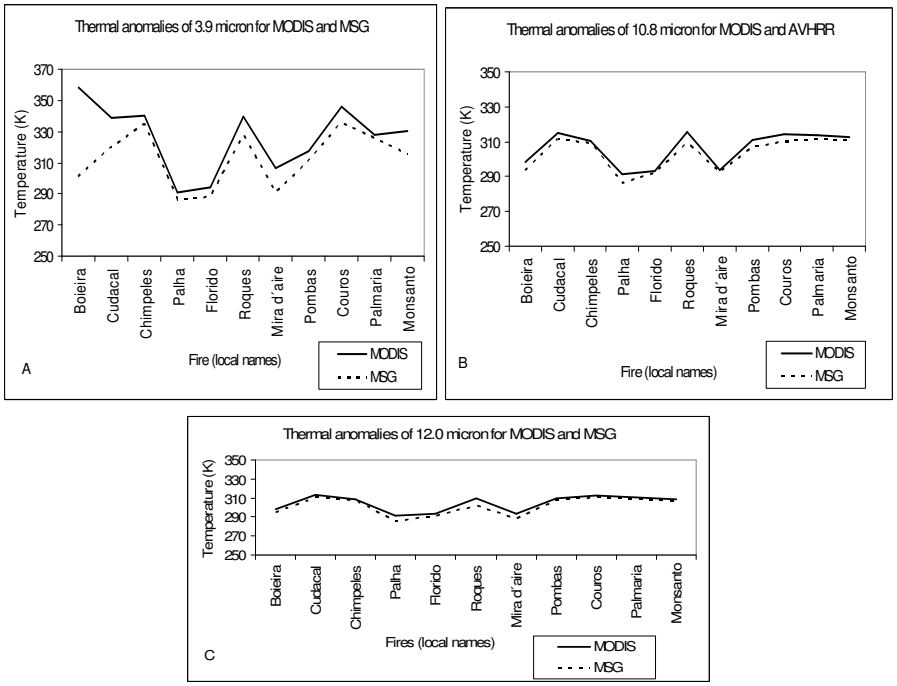

Figure 4.22 Comparing thermal anomalies for MSG and MODIS, (A) 3.9 micron (B) 10.8 micron (C) 12.0 micron

Figure 4.22 compares the thermal anomaly for MODIS and MSG for 11 fires. The temperature of the fire pixels of MODIS is higher than that of MSG for 3.9 µm, 10.8 µm and 12.0 µm. The temperature difference between MODIS and MSG for 3.9 µm is larger for large fires and hot fires having brightness temperatures higher than 335 K, this is because MSG 3.9 µm saturates at 335 K. The difference is not so large for

10.8 µm and 12.0 µm since their saturation temperature is 335K for MSG and even if the fires are very large they rarely reach that temperature.
Figure 4.23 shows the agreement between the 3 sensors in thermal anomaly detection for the same fire pixels. The correlation is high (0.91) comparing MODIS and MSG and high too for MSG and AVHRR comparison (0.80).

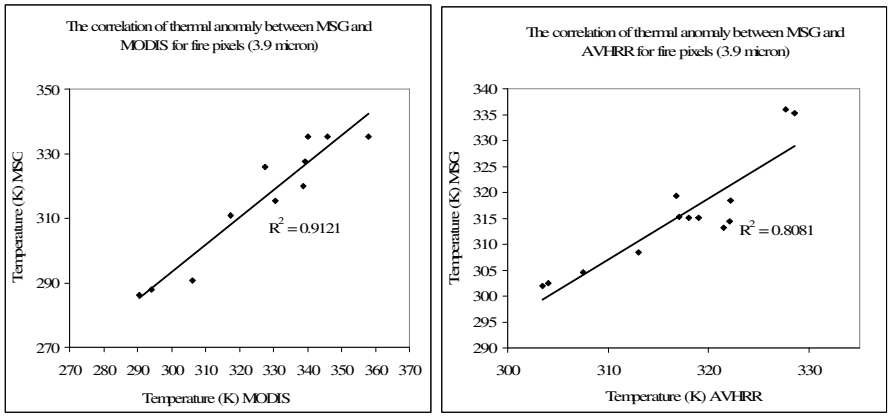

Figure 4.23 Correlation of the 3 sensors in thermal anomaly detection for the same fire pixels.

4.4.2 Comparing the performance of detecting fires

Table 4.3 gives an overview of the performance of the 3 sensors for fire detection**.** It does not seem a fair comparison due to the fact that the 3 sensors did not have the same number of images to be tested for fire detection due to their different temporal resolutions.

Table 4.3 overview of the performance of the 3 sensors for fire detection

	DETECTED FIRES			
ACTUAL FIRES	**MSG**			
		YES	NO	Total fires tested
	YES	22	3	25
	NO	0		
	MODIS			
	YES	9	5	14
	NO	0		
	AVHRR			
	YES	9	15	24
	NO	1		

Table 4.4 Statistics on the performance of MSG, MODIS and AVHRR

	MSG	MODIS	AVHRR
Errors of omission (%)	12	36	62
Errors of commission (%)	0	0	20
Fires detected (%)	88	64	37

Table 4.4 lists the errors of commission and omission for the 3 sensors in this research. It would have been preferred if there were more images tested, however field data for validation were available for just 27 fires. Further the disadvantage of the poor temporal resolution of the polar orbiting satellites led to acquisition of fewer images due to non-availability of an image during the fire time.

4.4.3 Analysis of the performance of the sensors

(a) The influence of solar zenith angle

All other conditions remaining constant a fire would be prominent as compared to its background at a larger solar zenith angle than at a smaller solar zenith angle. A smaller zenith angle would be a benefit for small fires on a cooler day, but on hot day with the non-fire pixel temperature also being high the smaller zenith angle increases the 3.9 temperature, leading to large false alarms.

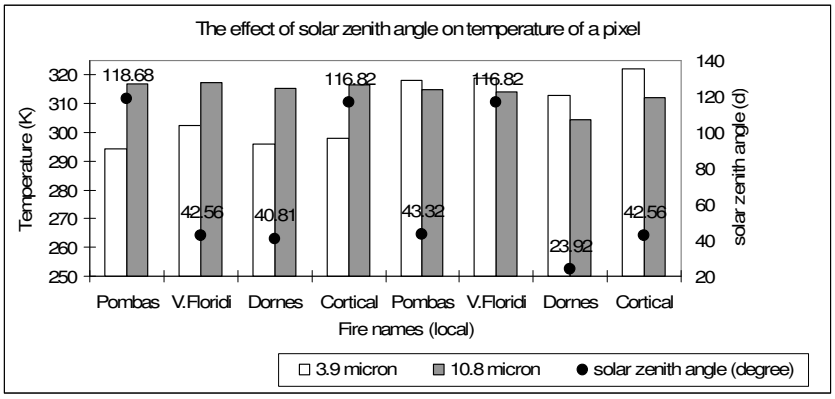

Figure 4.24 The influence of solar zenith angle on the temperature of fire pixel (AVHRR sensor)

Figure 4.24 shows the brightness temperatures of the fires along with the solar zenith angle for different NOAA satellites overpasses for the same fire. In the first sequence in order from the left (Pombas V. Florido, Dornes and Cortical) the solar zenith

angle is larger than the second sequence of the same fires; therefore the temperature of 3.9 µm is much lower than 10.8 µm. The reverse is seen with 3.9 µm being higher than 10.8 µm when the solar zenith angle is lower in the second sequence. Table 4.5 maybe referred for details on the satellite number or ID, date and time of the satellite overpass and solar zenith angle for the fires in figure 4.24.

Table 4.5 Satellite ID, date, time of overpass, solar zenith angle (AVHRR)

Fire (local names)	Overpass time (GMT)	Overpass date (D/M/Y)	NOAA ID	Solar zenith angle (^{o})
Pombas	20:58-22:43	09/08/2006	17	118.68
Florido	16:48-18:38	09/08/2006	15	70.17
Dornes	15:36-17:21	26/07/2006	15	67.47
Cortical	20:27-22:13	06/08/2006	17	116.82
Pombas	13:47-15:32	09/08/2006	16	43.32
Florido	13:47-15:32	09/08/2006	16	43.32
Dornes	13:09-14:54	26/07/2006	16	23.92
Cortical	14:30-16:07	06/08/2006	16	42.56

(b) The influence of scan angle

With increasing scan angle the pixel area increases and therefore the apparent brightness temperature decreases for the pixels. This is a disadvantage incase of AVHRR since the algorithm demands a certain difference in temperature between the 3.9 µm and 10.8 µm, and increasing scan angle affects 3.9 µm more than 10.8 µm. Even though the brightness temperature of fires is larger for MODIS than MSG for all fires yet many fires do not fulfill the conditions in the test since the 3.9 µm is affected drastically by these effects. Therefore fire pixels at 3.9 µm when compared with fire pixels in 10.8 µm or the non-fire background pixels (as in the thresholding algorithm condition) do not stand out as fire pixels. It was not possible to reduce the thresholds because it led to a large number of false alarms.

(c) The influence of saturation temperatures

Comparing the saturation temperatures of the 3.9 µm band in other words the most suitable band for fire detection, it maybe said that AVHRR has the lowest saturation temperature as mentioned before. Further AVHRR band 3b is at a shorter wavelength (3.7 µm) than the MODIS channel 21 and 22 (3.9 µm) and MSG channel 4 (3.9 µm), therefore it is more influenced by solar radiation. This leads to a large number of false alarms in case of AVHRR fire detection. This problem does not arise in case of MODIS and MSG which have a high saturation temperature. The low

saturation temperature of AVHRR makes it more vulnerable to solar zenith angle influences and scan angle influences.

4.4.4 The sensor best suited for fire detection

Based on the discussions in the previous sections it would be wise to decide that among the 3 satellites used in this research MSG SEVIRI satellite is the best suited for fire detection. Summarising the various themes explained above would make this decision more clear.

- Temporal resolution

The greatest advantage of MSG SEVIRI satellite as compared to MODIS and AVHRR is its temporal resolution. The satellite images a particular point of the Earth every 15 minutes. This is very vital for studying dynamic phenomena like detecting and monitoring of fire in real-time. The AVHRR and MODIS satellite sensors had the problem of not having images for certain fires. The added problem was that of clouds during the satellite overpass or of thick smoke due to fire during a particular overpass. Even if images were available the maximum was 2 incase of MODIS (Terra and Aqua) and a few more incase of AVHRR due to the various NOAA satellites (15, 16, 17, 18).

- solar zenith angle and scan angle of the sensor

The scan angle of the sensor is always the same for MSG unlike the polar orbiting satellites. MSG has a higher saturation temperature than AVHRR and hence not affected drastically by solar zenith angles. AVHRR is affected the most by solar zenith angle since 3.7 µm has a low saturation temperature (K) and a large number of pixels are flagged as fires.

- The saturations levels of the sensor
- The MSG has a higher saturation level than AVHRR.

The saturation level of MSG band 3.9 µm is same as MODIS band 22 (3.9 µm) but lower than band 21 (3.9 µm). MODIS band 21 is very noisy and is less preferred for fire detection.

- Spatial resolution

The spatial resolution of the polar orbiting satellites is higher than MSG and therefore leading to higher brightness temperature. As observed in this study the temperature of MSG was lower for fire pixels than the polar orbiting satellites, but the difference was not very large. Even though the spatial resolution of MSG was coarser yet MSG performed better in detecting fires since it was not affected by scan angle.

- Spectral coverage

In terms of spectral coverage the 3.7 µm band of AVHRR which is the most suitable band for fire detection is located close to the water vapour absorption wavelength. Being at a shorter wavelength it is more noisy than 3.9 µm band used for fire detection incase of MSG and MODIS causing a large number of false alarms due to high reflected solar radiation. The research detected fires incase of MODIS and MSG by differencing the thermal anomalies of most sensitive bands (3.7-4 µm) and least sensitive band (13.4 µm). Channel 5 (12 µm) of AVHRR is the band having the longest wavelength, this band could not be used as a substitute of 13.4 µm. Therefore, 3.7 µm of AVHRR was differenced with 11 µm and this did not give good results.

On the basis of the above arguments it maybe said that MSG and MODIS are better suited for fire detection than AVHRR. A high temporal resolution is a necessity for fire detection in near real time. MODIS has a very poor temporal resolution as compared to MSG therefore MSG SEVIRI stands out as the best sensor in this research for detecting forest fires.

4.5 SUMMARY

In chapter 4 the results of the field work data was depicted in a table and in a map. The results of the thermal anomaly detection incase of MSG, MODIS and AVHRR were presented. The 3.9 µm proved itself to be most suitable for detecting forest fires. The maps showing the fire pixels (MSG, MODIS and AVHRR were validated with the field data. The MSG detected the largest number of fires followed by MODIS and AVHRR. MSG also had the least error of commission and omission. On comparing the 3 sensors it was seen that MSG was more suitable for detecting forest fires.

5 CONCLUSIONS AND DISCUSSIONS

Fire detection in near real-time is very essential as it prevents losses of the environment and losses of man. This thesis developed an approach for detecting forest fires in near real-time by using polar orbiting and geostationary satellite observations. The performance of 3 sensors was compared. Answering the research questions the specific conclusions maybe summarised as followed:

5.1 SPECIFIC CONCLUSIONS

1. **The most suitable bands for detecting forest fires (MSG, MODIS, AVHRR)**

The most suitable bands for fire detection incase of the 3 sensors are the bands in the short wave infrared part of the electromagnetic part of the spectrum. Incase of MSG the channel 4 at 3.9 µm is most suitable for fire detection; incase of MODIS channel 21, 22 and 23 at 3.9-4 µm is most suitable for fire detection and for AVHRR it is channel 3b at 3.7 µm. But these bands cannot be used alone for fire detection and need to be compared or differenced with the least responsive band to fire which is the band at the longest infrared wavelength (13.4-13.9 µm).

2. **Developing a thresholding algorithm for MSG SEVERI, MODIS and AVHRR for detecting active fires (in near real-time)**

This research developed a method to detect active fires for each satellite sensor (MSG, MODIS, and AVHRR). The underlying approach for the 3 sensors was the same: Fires were detected by observing the TOA brightness temperatures. The following conclusions were drawn related to developing a method for fire detection.

2.1) Forest fire detection by observing TOA brightness temperature anomalies are appropriate for fire detection since forest fires are usually large fires yielding large anomalies in the fire pixel as compared to the surrounding pixels and so they can be easily distinguished. Therefore, knowledge of surface temperatures are not necessary and fire detection with TOA brightness temperatures is possible and this has given good results. Further it is difficult and a long drawn task to measure surface temperatures since knowledge of the emissivity of different surfaces are necessary which would lead to a delay in real-time fire detection.

2.2) In this research fire is detected by comparing the observed temperature with the expected temperature during a fire. The temperature expected during a fire is developed by a series of observations and the end product is a few thresholding algorithms stating the conditions to be maintained as expected during a

fire. The research has shown an approach for fire detection by applying a differential thresholding algorithm. The method that has been applied here for fire detection has shown good results for MSG, and not very satisfactory results for MODIS and AVHRR, but that is due to the peculiar characteristics of MODIS and AVHRR satellite sensors. On comparing the MODIS results of this research with the MODIS product it is seen that the results are comparable and the performance of both are equally unsatisfactory. MSG had performed far better than the MODIS product. AVHRR has performed worse than the MODIS product.

2.3) The fires that have been detected are quite precise in terms of the location as compared to the fire locations acquired during field work. Incase of MSG the fire flagged pixels overlap very accurately with the ground truth fire locations. Since the pixel size of MSG is 3 km and the entire pixel is flagged as fire therefore it is not possible to know the exact fire point. There was small shifts (maximum 100 meters) incase of MODIS, but these shifts were associated with the MODIS georeferencing. There were also small shifts in AVHRR flagged fire pixels. Therefore, the hypothesis is confirmed that forest fires can be detected precisely with TOA brightness temperatures.

3. Comparing the performance of MSG, MODIS and AVHRR in detecting forest fires

On comparing the performance of the 3 sensors it was seen that MSG was the most suitable for fire detection since it has a better temporal resolution than MODIS and AVHRR, it is not affected by the ill effects of scan angle and solar zenith angle, it has a higher saturation temperature than AVHRR and same as MODIS channel 22 and 23 (3.9-4 micron). In this research MSG has flagged the largest number of fires (88%) with an omission rate of 12%. The null hypothesis has been confirmed that MSG has better capabilities for fire detection than MODIS and AVHRR.

5.2 LIMITATIONS OF RESEARCH

1. Constant threshold set for all areas not taking into consideration the local variations in the temperature of the area.

The temperature differs according to relief, slopes facing the sun and local factors. This could cause false alarms of incase of hot objects in relatively cooler places and omission of small fires in relatively hotter places. It was not possible to apply different thresholds for different locations in Portugal since data regarding the local weather conditions were not available. The research tried to overcome this problem

by developing a large fires threshold test and a small fires threshold test, but this is not necessary if the normal local temperature conditions are known.

2. The algorithm is not tested for all seasons

Since majority of the fires in Portugal occur during July, August and September therefore, the algorithm was tested only for fires in these months. The thresholds would have to be tuned to the temperature conditions of different months.

3. The test was applied to all pixels regardless of the landcover types therefore the likelihood for false alarms was greater.

Bare soil and rock show high temperatures as compared to vegetated or forest areas during summer and could be a cause for false alarms. It would have been better to apply the algorithms to only the forest pixels. But since Portugal has very frequent fires and the forested areas are not regularly mapped it was not possible to get this data. Cloud contamination of the pixels was also a problem since a cloud mask was not used.

4. Accuracy of the exact coordinates of the fire area

The pixel size of the sensors used in this research is coarse and the entire pixel is flagged as fire therefore, it might lead to some delay in finding the exact point of fire during time of emergency. Atmospheric corrections have not been done therefore there might be shifts in the actual positions of the fire especially if it is a windy day. Such shifts were however not noticed in this research.

5. Exclusion of centre fire pixel in case of the Contextual algorithm

Incase of the contextual algorithm where the temperature of the fire pixel is compared to the background temperature, it may lead to omission of a fire pixel surrounded by other fire pixels, since the centre fire pixel would not fulfill the condition of the algorithm. Figure 40 shows the limitation of the contextual algorithm. This problem did not arise in the research since when the command '*nbmin*' was used the fire pixel temperature was compared with the minimum of its neighbour temperature in all directions (right, left, top, bottom and diagonally). The fire would have to be larger than 8100 (ha) to fulfill this condition incase of MSG pixels; incase of MODIS and AVHRR the fire would have to be larger than 900 (ha) in area. The problem might arise for extremely large fires or a group of very close fires when the surrounding pixels are flagged as fires and the centre pixel is not flagged, in this case it should be assumed that the centre pixel is a fire.

fire	fire	fire
fire	No fire	fire
fire	fire	fire

Figure 4.25 limitation of contextual algorithm

5.3 RECOMMENDATIONS

1. Masking the vegetated pixels

Areas devoid of vegetation may show high temperatures in summer and produce false alarms therefore, it is best to apply the thresholding algorithm only on forest areas. This would solve the problem of omissions and commissions since then the threshold can then be lowered. The masking might also help in knowing the precise location of the fire when a large pixel such as 3km is flagged as fire.

2. Masking cloud pixels and water pixels

Cloud and water pixels also create the problem of false alarms. Clouds show fire like properties in many instances but if a good cloud mask is used it could solve the problem.

3. Manipulating the threshold levels

The fixed threshold algorithm would work better if the threshold levels are changed locally according to the weather conditions of the area.

As concluding remarks the author would like to say that there are presently no algorithms which can be used globally due to the different weather conditions and sensor characteristics, and same is the case for the algorithms developed in this research. However, the same method can be applied to all areas after manipulating the threshold values. The above recommendations must be considered for the algorithm to work better for detecting forest fires. Polar orbiting satellites have a higher spatial resolution than geostationary satellites but there is a problem in acquiring continuous images for the fires, whereas geostationary satellites like the MSG SEVIRI provides images every 15 minutes. It would have been good if there were a large number of polar orbiting satellites operating and therefore a particular place would get many images throughout the day, then a combination of polar orbiting and geostationary satellites could have been used for detecting and monitoring dynamic phenomenon like forest fires. However since at present this is not the case therefore it maybe mentioned that geostationary satellites are more suitable than polar orbiting satellites for real-time detecting and monitoring a dynamic phenomenon like forest fires.

6. REFERENCES

Gieske, A.S.M., Hendrikse, J., Retsios, V., Leeuwen, B. V., Maathuis, B.H.P., Romaguera, M., Sobrino, J.A., Timmermans, W.J., Su, Z., (2004), Processing of MSG-1 SEVERI data in the thermal infrared algorithm development with the use of the sparc2004 data set. URL: www.itc.nl/library/papers_2005/conf/gieske_pro.pdf [accessed 2006, December 18]

Arino, O., & Melinotte, J.M., (1998), Cover the 1993 Africa Fire Map *International Journal of Remote Sensing,* 19**,** 2019-2023

Aster Homepage URL: http://asterweb.jpl.nasa.gov [accessed 2006, December 07]

Ayanzi, J. S. M., Ravail, N., Kelha, V., & Ollero, A., (2005), Active Fire Detection for Fire Emergency Management: Potential and Limitations for the Operational Use of Remote Sensing. *Natural Hazards,* 35**,** 361–376

Cihlar, J., Belward, A., & Govaerts, Y., (1999), Meteosat Second Generation Opportunities for Land Surface Research and Applications. In EUMETSAT (Ed.) *EUMETSAT Scientific Publications.* Germany

Direcção Geral Dos Recursos Florestais, DGRF (2006), *Incêndios Florestais* 2006, report 17 October 2006. [Received from government organization on 2006 2nd January]

Encyclopaedia Britannica article, Portugal land. URL: http://www.britannica.com /eb/article-23787/Portugal [accessed 2006 December 17]

EUMETSAT AND CGMS (1999), Directory of Meteorological Satellite Applications. URL: http://www.wmo.ch/web/sat/en/ap2-11.htm [accessed 2007, January 01]

EUMETSAT Homepage URL: http://www.eumetsat.int [accessed 2006, November 13]

European Commission (2001), Report N0.1: Forest fires in Southern Europe. In Ayanz, J.S.M., Barbosa, P., Schmuck, G., & Schulte, E., (Ed.), Official Publication of the European Communities, SPI.01.95.EN.

European Commission (2003a), The European Forest Fires Information System (EFFIS) results on the 2003 fire season in Portugal by the 20th of August. In Schmuck, G., Miguel-Ayanz, J. S., Barbosa, P., Camia, A., Kucera, J., Libertá, G., (Ed.)

European Commission (2003b), Forest Fires in Europe - 2002 fire campaign IN J. San-Miguel-Ayanz, J., Barbosa, P., Libertà, G., Schmuck, G., & Schulte, E., (Ed.), Official Publication of the European Communities, SPI.03.83.EN.

European Commission (2004), Forest Fires in Europe - 2003 fire campaign. In San-Miguel-Ayanz, J.S., Barbosa, P., Camia, A., Kucera, J., Libertà, G., Schmuck, G., Schulte, E., Bucella, P., Colletti, L., & Flies, R., (Ed.), Official Publication of the European Communities, SPI.04.124 EN.

European Commission (2005), Forest Fires in Europe 2004. In Schmuck, G., San-Miguel-Ayanz, J., Barbosa, P., Camia, A., Kucera, J., Libertá, G., (Ed.), Official Publication of the European Communities, S.P.I.05.147 EN

European Commission (2006a), The European Forest Fire Information System Newsletter URL: http://effis.jrc.it/documents/2006/EFFIS_Newsletter-2006_01.pdf [accessed 2006, November 13]

European Commission (2006b), Forest fires in Europe 2005. In Schmuck, G., Miguel-Ayanz, J. S., Barbosa, P., Camia, A., Kucera, J., Libertà, G., Schulte, E., Colletti, L., Martin, H., Toussaint, M., (Ed.), Official Publication of the European Communities, EUR 22 312 EN.

Giglio, L., Descloitres, J., Justice, C.O., & Kaufman Y.J., (2003), An Enhanced Contextual Fire Detection Algorithm for MODIS. *Remote Sensing of Environment,* 87**,** 273-282.

Giglio, L., Kendall, J.D., & Justice C.O., (1999), Evaluation of global fire detection algorithms using simulated AVHRR infrared data *International Journal of Remote Sensing,* 20**,** 1947-1985.

Global Fire Monitoring Centre (GFMC) / Fire Ecology Research Group, The Canadian forest fire weather index (FWI) system URL: http://www.fire.uni-freiburg.de/fwf/ca_fwi.htm [accessed 2007 January 7]

Goodrum, G., Kidwell, K.B., & Winston, W.,(2000), NOAA KLM User's guide. In U.S. Department of Commerce National Oceanic and Atmospheric Administration National Environmental Satellite, D., and Information Service (Ed.). URL: http://www2.ncdc.noaa.gov/docs/klm/ [accessed 2006, November 10]

Instituto de Metreologia, Fire Risk Index (FWI) URL: http://www.meteo.pt/en/previsao/riscoincendio/risc_incend_fwi.html [accessed 2007 January 7]

Instituto de Meteorologia, I.P. Portugal, (2006a), *Apoio meteorologico na prevencao E combate de incendios florestais, relatorio final epoca 2006*. Report acquired by government official on 2006 January 10.

Kaufman, Y.J., Justice, C., Flynn, L., Kendall, J., Prins, E., Ward, D.E., Menzel, P., & Setzer, A., (1998) Monitoring Global Fires from EOS-MODIS. *Journal of Geophysical Research,* Volume 103**,** p. 32215-32338

Kerle, N., Janssen, L.L.F., & Huurnemann, G.C., (2004), *Principles of remote sensing* 3rd edition, ITC Enschede, The Netherlands.

LANDSAT Homepage URL: www.landsat.org [accessed 2006, December 07]

Li, Z., Nadon, S., & Cihlar, A.J., (2000), Satellite-based detection of Canadian boreal forest fires: development and application of the algorithm. *International Journal for Remote Sensing,* 21**,** 3057-3069.

Lim, A., Chin, S., Lim, K., & Kwoh, L., (2001), Computation of sub pixel fire temperature with MODIS data. In Centre For Remote Imaging, S. A. P. C., National University of Singapore; Singapore Institute of Surveyors and Valuers (SISV); Asian Association on Remote Sensing (AARS) (Ed.) *22nd Asian Conference on Remote Sensing, 5-9 November 2001.* Singapore.

National Aeronautics and Space Administration (NASA) MODIS Web URL: http://modis.gsfc.nasa.gov/about/media.php [accessed 2006, November 13]

Prins, E. M., Mcnamara, D., & Schmidt, C. C., (2004), Global Geostationary Fire Monitoring System. *13th Conf. on Satellite Meteorology and Oceanography.* Norfolk, VA, Amer. Meteor. Soc., P4.6.

Schmetz, J., Pili, P., Tjemkes, S., Just, D., Kerkmann, J., Rota, S., & Ratier, A., (2002), An Introduction to Meteosat Second Generation (MSG). *Bulletin of the American Meteorological Society,* 83**,** 977-992.

Stroppiana, D., Pinnock, S., & Gregoire, J.M., (2000), The Global Fire Product: daily fire occurrence from April 1992 to December 1993 derived from NOAA AVHRR data. *International Journal of Remote Sensing* Volume 21**,** 1279 – 1288

Van Den Bergh, F. & Frost, P. E., (2005), A multi temporal approach to fire detection using MSG data. *Analysis of Multi-Temporal Remote Sensing Images, 2005 International Workshop on the***,** 156-160.

Wolfe, R. E., Nishihama, M., Fleig, A. J., Kuyper, J. A., ROY, D. P., Storey, J. C. & Patt, F. S. (2002), Achieving sub-pixel geolocation accuracy in support of MODIS land science. *Remote Sensing of Environment,* 83**,** 31-49

Wikipedia (2006), Geography of Portugal, URL: http://en.wikipedia.org/wiki/Geography_of_Portugal [accessed 2006 December 17]

Wikipedia, the free encyclopedia, 2006a, Santarem, Portugal, URL: http://en.wikipedia.org/wiki/Santar%C3%A9m,_Portugal [accessed 2006 December 17]

Wikipedia, the free encyclopedia, 2006b, Leiria URL: http://en.wikipedia.org/wiki/Leiria [accessed 2006 December 17]

7. APPENDICES

Appendix 1 Calculating radiances and temperatures (MSG SEVIRI)

The radiance is calculated by

$$L_{wn} = slope * DN + offset$$

Where L_{wn} is the radiance in [$mWm^{-2}sr^{-1}(cm^{-1})^{-1}$]; DN is the digital number (10 bit)
The slope and offset are retrieved from the header files;
The brightness temperatures are calculated by the following formula

$$T_b = \left[\frac{c_2 v_c}{\log\left(\frac{c_1 v_c^{\ 3}}{R^{+1}} \right)} - B \right] / A$$

T_b is the brightness temperatures (K); R is the observed radiances in [$mWm^{-2}sr^{-1}(cm^{-1})^{-1}$]; v_c is the central wave number of the channel. The radiation constants are given by [$c_1 = 2hc^2$ and $C_2 = hc/k_B$.]; c is the velocity of light, k_B is Boltzmann's constant and h is Planck's constant.

Table 7.1 Example of radiance and temperature calculation (MSG 3.9 µm)

STEPS	**VALUES**	**UNITS**
Radiance Conversion= offset + (DN*slope		
DN (2^{10}) 0-1023	**300**	Dimensionless
slope	0.00366	(W/m2/micrometer/sr
offset	-0.18659	Dimensionless
radiance	**0.91141**	W/m2/micrometer/sr
Temperature Conversion= ((CC2)/ln(CC1+1))-b)/a		
(c1) (Planck constant)	c1= 0.0000119104	
(c2) (Planck constant)	c2= 1.438770000000	
vc	2569.094000000000	
a	0.995900000000	
b	3.471000000000	
CC2=c2*vc	3696.335374380000	
CC1=(c1*Vc^3)/R	221591.216824956000	
Temperature	**298.05627**	Kelvin

Appendix 2 Calculating radiances and temperatures (MODIS)

The image had values of calibrated radiances which were in integer format and were derived by the following formula.

$$[radiance = radiance\_scales(Interger - radiance\_offsets)]*1000000$$

The radiances are then converted to temperatures by the *Planck's radiation Law*.

$$T = \left(\frac{hc}{k\lambda}\right)\frac{1}{\ln\left(2hc^2\lambda^{-5}L^{-1}+1\right)}$$

L = radiance (Watts/m2/steradian/m)

h = Planck's constant (joule second) (6.63E-34)

c = speed of light in vacuum (m/s) (3.00E+08)

k = Boltzmann gas constant (joules/Kelvin) (1.38E-23)

λ = band or detector center wavelength (m)

T = temperature (Kelvin)

Table 7.2 Example of radiance and temperature calculation (MODIS 3.9 µm)

STEPS	VALUES	UNITS
Radiance Conversion [radiance (L) = scale * (integer value-offset)]		
Integer value (range 0 - 32767)	**30000**	Dimensionless
Scale (header)	6.92E-05	(W/m2/micrometer/sr
Offset (header)	2730.58	Dimensionless
radiance (L	1.88748017472	W/m2/micrometer/sr
radiance (L) in Meter	**1887480.175**	W/m2/meter/sr
Temperature Conversion [T= (hc/kλ)*(1/ln(2hc^{2}λ^{-5}L^{-1}+1))]		
Band 22 centre wavelength (λ)	3.964	micrometer
Band 22 centre wavelength (λ)	0.000003964	m
h Planck's constant	6.63E-34	Joule/second
c speed of light	3.00E+08	m/s
kB (Boltzmann gas constant)	1.38E-23	Joules/Kelvin
c1=2hc^2	1.1910427225432500000E-16	
c2=hc/kBWL	3.63E+03	
Temperature (Kelvin)	**327.7586867**	Kelvin

Appendix 3 Calculating radiances and temperatures (AVHRR)

The image had DN values in integer format. The DN was converted to radiance by the following formula:

$$\text{Radiance (Ne)} = a_0 + a_1 * CE + a_2 * CE^2$$

Where CE is digital number; a_0, a_1 and a_2 are thermal coefficients derived from the header file. The temperature T_1 (Kelvin) is calculated with the following formula

$$T_1 = \frac{c_2 vc}{\ln\left(1 + \frac{c_1 v^3}{NE}\right)}$$

The corrected temperature is calculated by the following formula:

$$T_2 = \frac{T_1 - A}{B}$$

Where c_1 and c_2 are the Plank radiation constants; vc is the centroid wave number

Table 7.3 Example of radiance and temperature calculation (AVHRR 12.0 µm)

STEPS	VALUES	UNITS
Radiance Conversion [Radiance (Ne) = $A_0+A_1*CE+A_2*CE^2$]		
CE (DN) (2^{10}) 0-1023	**407**	
Thermal coefficients for band 5 AVHRR (12.0µm)		
A_0	197.6508640	
A_1	-0.2111840	
A_2	0.0000126	
Radiance (Ne) =	**113.7861534**	mW/(m^2-sr-cm^{-1})
Temperature Conversion [$T_1= c_2vc/(\ln(1+(c_1v^3/NE)))$]		
vc	839.8246000	(cm^{-1})
Planck's Radiation Constants (C_1, C_2)		
C1	1.19104E-05	mW/(cm2/sr/cm-4)
C2	1.4387752	cm K
T_1	291.6417049667090000	Kelvin
$T_2 = (T_1-A/B)$		
A (from header)	0.3091800	
B (from header)	0.9990120	
T_2	**291.9511907**	Kelvin

There is an inverse relationship between DN and radiance incase of AVHRR/3 images. The higher is the DN the lower is the radiance and vice versa. Incase of MODIS and MSG the relationship between DN and radiance is proportional.

Appendix 4 ILWIS scripts used for applying algorithms for fire detection

1. MSG Absolute thresholding

```
Test1= t039-t134
Test2= t039-t134
Test3=iff((Test1-Test2>5)and(Test1>35)and(VIS006<=0.15),1,0)
```

Where, t is temperature; 039 is 3.9 µm, 134 is 13.4 µm and vis06 is 0.6 µm. In Test1: Difference between 3.9 µm and 13.4 µm is calculated for the 'fire pixel on the fire day'. In Test2: Mean difference between 3.9 µm and 13.4 µm is calculated for the 'same fire pixel on previous 10 non-cloudy days'. In Test3: 'iff' is a Boolean expression in the ILWIS software. The command claims that if the various conditions in brackets are fulfilled then the value of the output pixel should be '1' or else '0'.

2. MSG Contextual thresholding

```
Test1= iff(039-nbmin(039#)>10,039-nbmin(039#),0)
Test2= iff((039-134>30)and(039>315)and(VIS006<=0.15),Test1,0)
```

Where, t is temperature; 039 is 3.9 µm, 134 is 13.4 µm and vis06 is 0.6 µm; 'nbmin' is a neighbourhood operation in the ILWIS software. In Test2 command claims that if the various conditions in brackets are fulfilled then let the output be 'Test1' or else a '0'.

3. MODIS large threshold algorithm

```
Test1= iff(t20-nbmin(t20#)>20,t20-nbmin(t20#),0)
Test2= iff((t20>350)and(t20-t36>100)and(VIS006<=0.2),Test1,0)
```

Where, t is temperature, 20 is band 20 (3.7 µm); 36 is band 36 (13.6 µm); VIS006 is band 1 (0.6 µm). The same commands are used for band 21 (3.9 µm) and band 22 (3.9 µm), only the image name is changed. The same commands are used for the small fires threshold test, only the values are changed.

4. AVHRR threshold algorithm

```
Test1= iff(t3-nbmin(t3#) > 20, t3-nbmin(t3#), 0)
Test2= iff((t3-t4>10) and (t3>315) and (T4>300), Test1, 0)
Test3= iff((R1<=0.1) and (R2-R1<=0.1), Test2, 0)
```

Where, t is temperature; 3 is band 3 (3.7 µm); 4 is band 4 (11 µm); R1 is band 1 (0.6 µm) and R2 is band 2 (1.1 µm).

Appendix 5 Thermal anomaly detection MSG (3.9 µm)

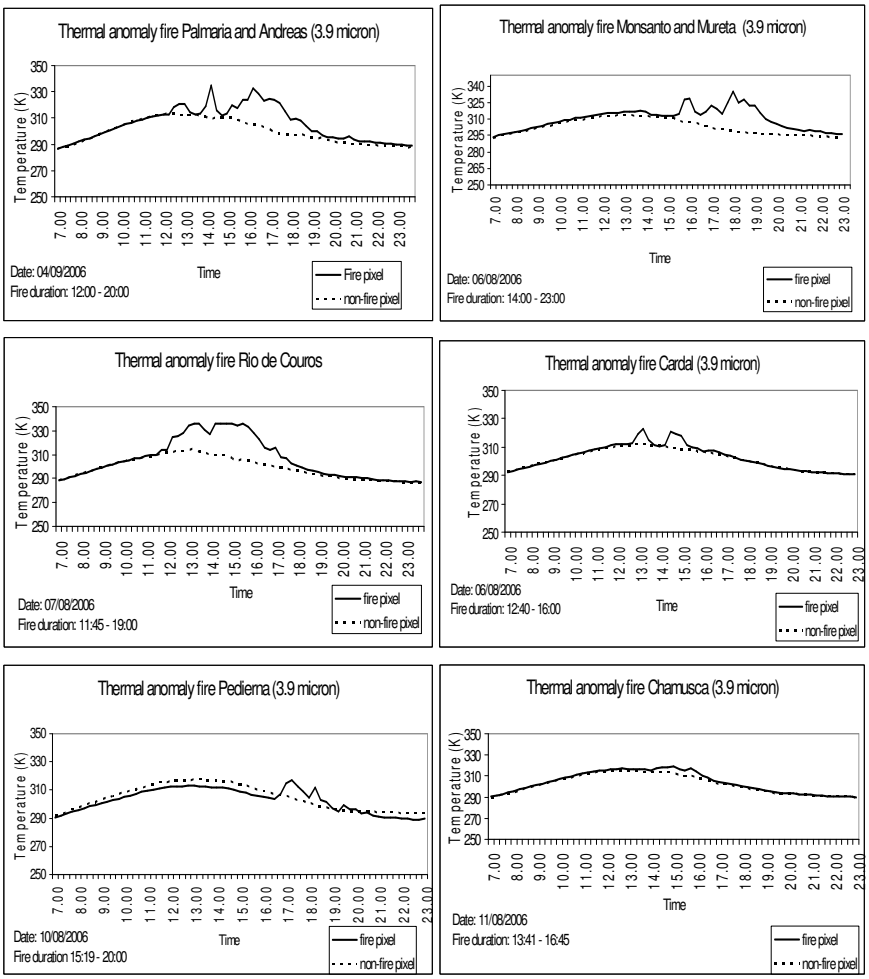

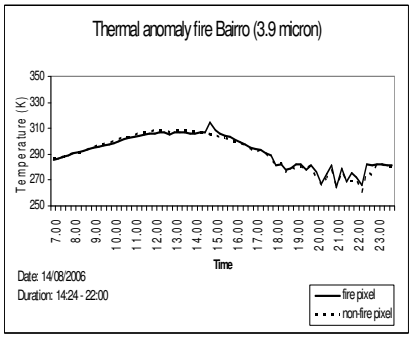
Thermal anomaly fire Bairro (3.9 micron)
Temperature (K)
Time
Date: 14/08/2006
Duration: 14:24 - 22:00
fire pixel
non-fire pixel

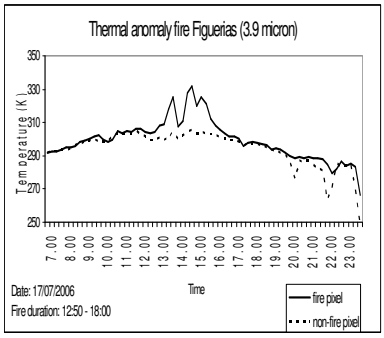
Thermal anomaly fire Figueiras (3.9 micron)
Temperature (K)
Time
Date: 17/07/2006
Fire duration: 12:50 - 18:00
fire pixel
non-fire pixel

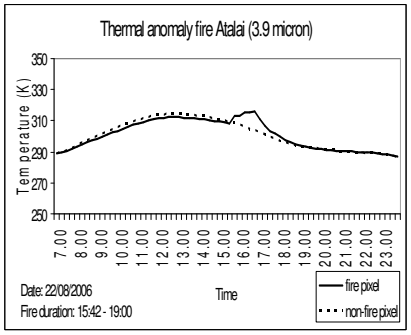
Thermal anomaly fire Atalai (3.9 micron)
Temperature (K)
Time
Date: 22/08/2006
Fire duration: 15:42 - 19:00
fire pixel
non-fire pixel

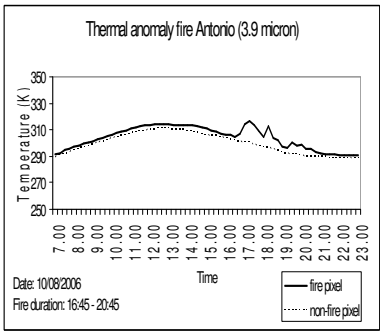
Thermal anomaly fire Antonio (3.9 micron)
Temperature (K)
Time
Date: 10/08/2006
Fire duration: 16:45 - 20:45
fire pixel
non-fire pixel

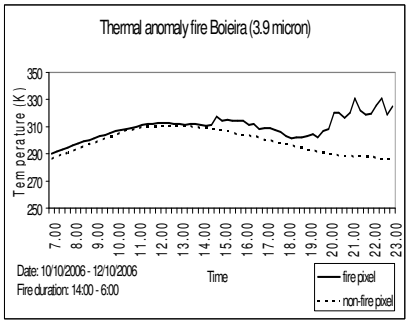
Thermal anomaly fire Boieira (3.9 micron)
Temperature (K)
Time
Date: 10/10/2006 - 12/10/2006
Fire duration: 14:00 - 6:00
fire pixel
non-fire pixel

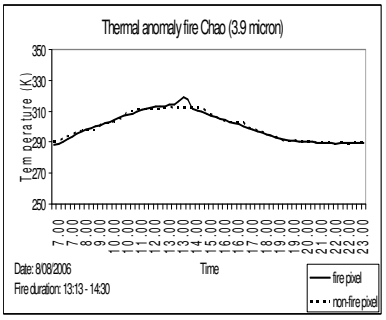
Thermal anomaly fire Chao (3.9 micron)
Temperature (K)
Time
Date: 8/08/2006
Fire duration: 13:13 - 14:30
fire pixel
non-fire pixel

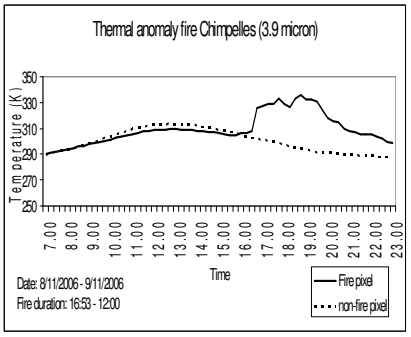
Thermal anomaly fire Chimpelles (3.9 micron)
Temperature (K)
Time
Date: 8/11/2006 - 9/11/2006
Fire duration: 16:53 - 12:00
Fire pixel
non-fire pixel

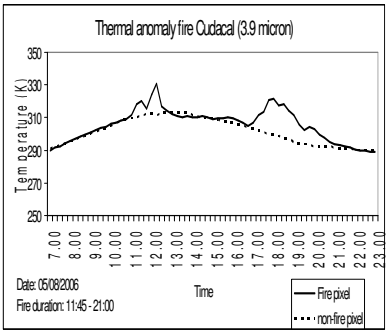
Thermal anomaly fire Cudacal (3.9 micron)
Temperature (K)
Time
Date: 05/08/2006
Fire duration: 11:45 - 21:00
Fire pixel
non-fire pixel

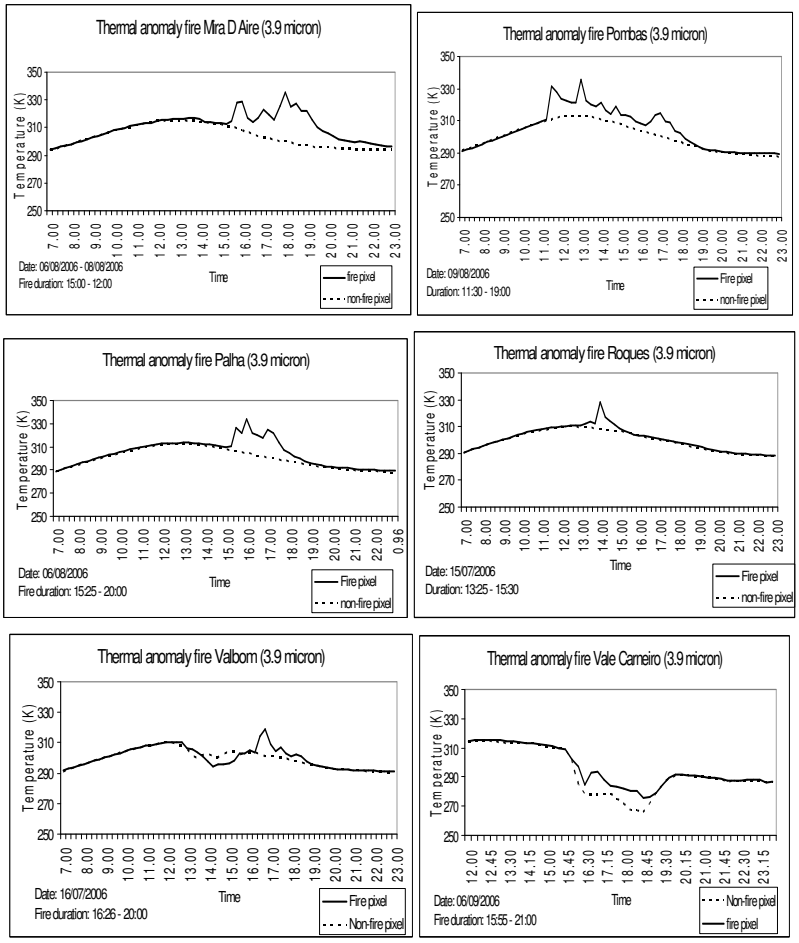

Appendix 6 Thermal anomaly detection MODIS thermal bands

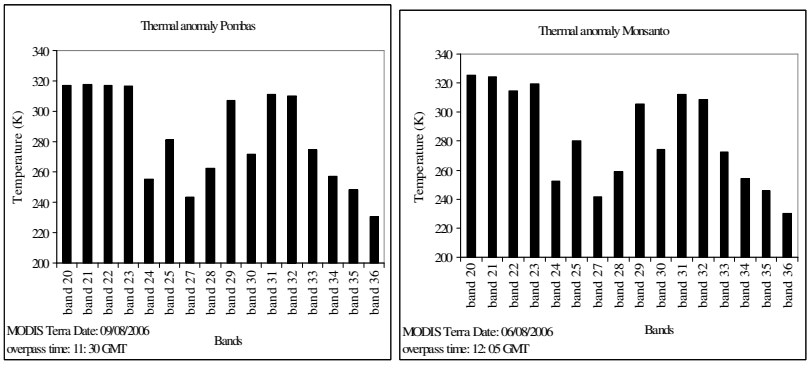

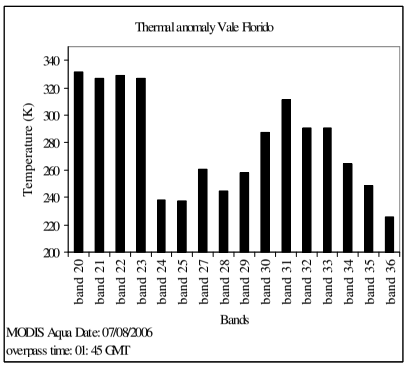
Thermal anomaly Vale Florido
Temperature (K)
340
320
300
280
260
240
220
200
band 20
band 21
band 22
band 23
band 24
band 25
band 27
band 28
band 29
band 30
band 31
band 32
band 33
band 34
band 35
band 36
Bands
MODIS Aqua Date: 07/08/2006
overpass time: 01: 45 GMT

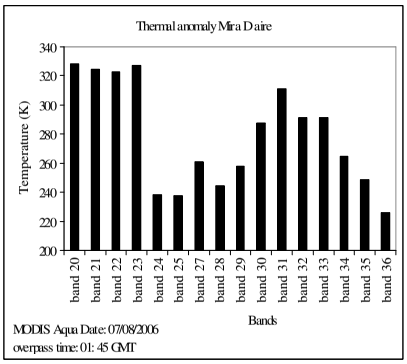
Thermal anomaly Mira Daire
Temperature (K)
340
320
300
280
260
240
220
200
band 20
band 21
band 22
band 23
band 24
band 25
band 27
band 28
band 29
band 30
band 31
band 32
band 33
band 34
band 35
band 36
Bands
MODIS Aqua Date: 07/08/2006
overpass time: 01: 45 GMT

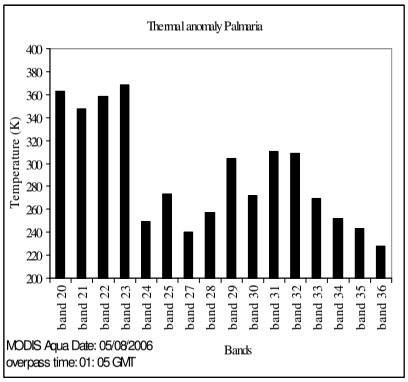
Thermal anomaly Palmaria
Temperature (K)
400
380
360
340
320
300
280
260
240
220
200
band 20
band 21
band 22
band 23
band 24
band 25
band 27
band 28
band 29
band 30
band 31
band 32
band 33
band 34
band 35
band 36
Bands
MODIS Aqua Date: 05/08/2006
overpass time: 01: 05 GMT

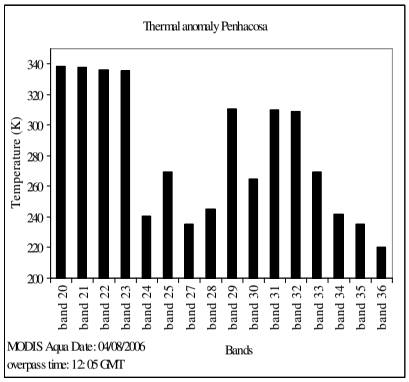
Thermal anomaly Penhacosa
Temperature (K)
340
320
300
280
260
240
220
200
band 20
band 21
band 22
band 23
band 24
band 25
band 27
band 28
band 29
band 30
band 31
band 32
band 33
band 34
band 35
band 36
Bands
MODIS Aqua Date: 04/08/2006
overpass time: 12: 05 GMT

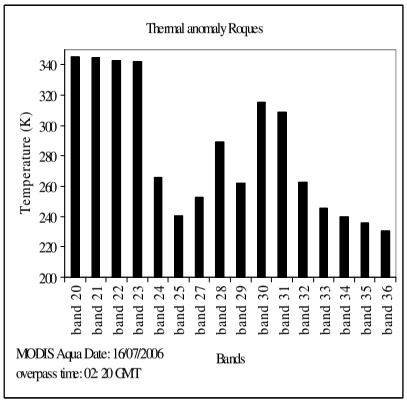
Thermal anomaly Reques
Temperature (K)
340
320
300
280
260
240
220
200
band 20
band 21
band 22
band 23
band 24
band 25
band 27
band 28
band 29
band 30
band 31
band 32
band 33
band 34
band 35
band 36
Bands
MODIS Aqua Date: 16/07/2006
overpass time: 02: 20 GMT

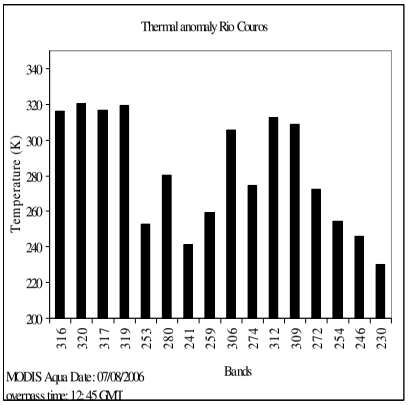
Thermal anomaly Rio Couros
Temperature (K)
340
320
300
280
260
240
220
200
316
320
317
319
253
280
241
259
306
274
312
309
272
254
246
230
Bands
MODIS Aqua Date: 07/08/2006
overpass time: 12: 45 GMT

Appendix 7 Thermal anomaly detection AVHRR thermal bands

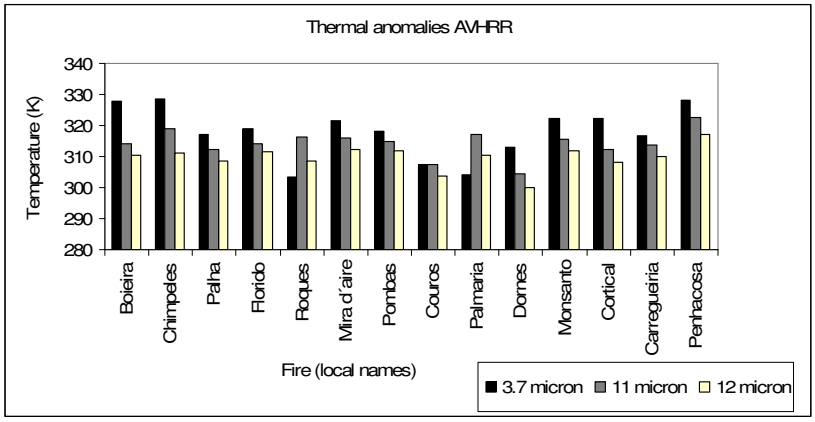

The NOAA satellites overpass date and time for appendix 7 fires

Fire (local names)	Overpass time (GMT)	Date of overpass (date/month/year)	NOAA ID
Boieira	02:27-04:22	11/08/2006	18
Chimpeles	16:19-17:40	11/08/2006	15
Palha	14:30-16:07	06/08/2006	16
Florido	13:47-15:32	09/08/2006	16
Roques	16.39-18:22	15/07/2006	15
Mira d´aire	14:30-16:07	06/08/2006	16
Pombas	13:47-15:32	09/08/2006	16
Couros	13:00-14:46	07/08/2006	16
Palmaria	16:24-18:09	04/09/2006	15
Dornes	13:09-14:54	26/07/2006	16
Monsanto	14:30-16:07	06/08/2006	16
Cortical	14:30-16:07	06/08/2006	16
Carregueiria	16:19-17:40	11/08/2006	15
Penhacosa	13.21-14:54	04/08/2006	17

Appendix 8 A few examples of the number of times a pixel is flagged as fire after applying the fire detection algorithm (Contextual) in case of MSG